Weak universality, quantum many-body scars, and anomalous infinite-temperature autocorrelations in a one-dimensional spin model with duality

Adithi Udupa,[1,*] Samudra Sur,[1,*] Sourav Nandy,[2] Arnab Sen,[3] and Diptiman Sen[1,4]
[1]*Center for High Energy Physics, Indian Institute of Science, Bengaluru 560012, India*
[2]*Jožef Stefan Institute, SI-1000 Ljubljana, Slovenia*
[3]*School of Physical Sciences, Indian Association for the Cultivation of Science, Jadavpur, Kolkata 700032, India*
[4]*Department of Physics, Indian Institute of Science, Bengaluru 560012, India*

(Received 2 August 2023; revised 22 November 2023; accepted 8 December 2023; published 26 December 2023)

We study a one-dimensional spin-1/2 model with three-spin interactions and a transverse magnetic field h. The model is known to have a $Z_2 \times Z_2$ symmetry and a duality between h and $1/h$. The self-dual point at $h = 1$ is a quantum critical point with a continuous phase transition. We compute the critical exponents z, β, γ, and ν, and the central charge c numerically using exact diagonalization (ED) for systems with periodic boundary conditions. We find that both z and c are equal to 1, implying that the critical point is governed by a conformal field theory with a marginal operator. The values obtained for β/ν, γ/ν, and ν from ED suggest that the model exhibits Ashkin-Teller criticality with an effective coupling that is intermediate between the four-state Potts model and two decoupled transverse field Ising models. A more careful analysis on much larger systems but with open boundaries using density-matrix renormalization group (DMRG) calculations, however, reveals important additive and multiplicative logarithmic corrections at and near criticality, and we present evidence that the self-dual point may be in the same universality class as the four-state Potts model. An energy level spacing analysis shows that the model is not integrable. For a system with an even number of sites and periodic boundary conditions, there are exact mid-spectrum zero-energy eigenstates whose number grows exponentially with the system size. A subset of these eigenstates have wave functions that are independent of the value of h and have unusual entanglement structures; hence these can be considered to be quantum many-body scars. The number of such quantum scars scales at least linearly with system size. Finally, we study the infinite-temperature autocorrelation functions at sites close to one end of an open system. We find that some of the autocorrelators relax anomalously in time, with pronounced oscillations and very small decay rates if $h \gg 1$ or $h \ll 1$. If h is close to the critical point, the autocorrelators decay quickly to zero except for an autocorrelator at the end site.

DOI: 10.1103/PhysRevB.108.214430

I. INTRODUCTION

The well-known transverse field Ising model (TFIM) in one dimension has been studied extensively over many years [1–3]. The Hamiltonian of the model consists of two-spin interactions (with strength set equal to 1) and a transverse magnetic field with strength h,

$$H_2 = -\sum_{j=1}^{L} \left[\sigma_j^z \sigma_{j+1}^z + h\, \sigma_j^x\right], \tag{1}$$

where σ_j^a denote the Pauli matrices at site j corresponding to a spin-1/2 degree of freedom, and we are considering a system with L sites and periodic boundary conditions (PBC). The model has a Z_2 symmetry since an operator $D = \prod_{j=1}^{L} \sigma_j^x$ commutes with the Hamiltonian. The model is known to have a quantum phase transition at a critical point given by $h = 1$. It has a ordered phase for $h < 1$ with a finite magnetization (the Z_2 symmetry is spontaneously broken in this phase), and a disordered phase for $h > 1$ with zero magnetization. It also exhibits duality [4,5] and the self-dual point $h = 1$ is the quantum critical point. The critical point is known to be described by a conformal field theory with $c = 1/2$ and certain critical exponents which are known analytically [6].

Generalizations of the TFIM with p-spin interactions with duality have been proposed [7] and studied using mean-field theory [8], finite-size scaling [9–11], and series expansions [12], with the TFIM corresponding to the case $p = 2$. It is of particular interest to take a close look at what happens in the next simplest case $p = 3$ where the order of phase transition in literature has been debated. We study this case numerically using exact diagonalization (ED) and look at the quantum criticality in this system at the self-dual point which is again given by $h = 1$. Another motivation for studying the case of $p = 3$ is that a Hamiltonian of this form may be engineered using optical lattices either with two atomic species [13] or with polar molecules driven by microwave fields [14]. We note that for the model with $p = 4$, it is not clear whether the transition at the self-dual point is first-order or continuous, while models with $p \geqslant 5$ are believed to have a first-order transition at the self-dual point [8,9,12].

The three-spin ($p = 3$) model is a candidate for interesting high-energy behavior as well. For an even number of spins and periodic boundary conditions (PBC), this model satisfies an index theorem [15] that results in the presence of an

*These authors contributed equally to this work.

exponentially large number (in system size) of exact mid-spectrum zero energy eigenstates. Since these states are degenerate in energy, any linear combination of these is also an eigenstate of the system. Recent works [16–20] have shown that this freedom allows for the possibility of creating mid-spectrum eigenstates which violate the eigenvalue thermalization hypothesis (ETH) by possessing very low entanglement entropy compared to the expected thermal entropy. These eigenstates can be classified as quantum many-body scars [21–28]. It would be interesting to see if the three-spin model hosts such scar states in the middle of the energy spectrum. Finally, we would like to examine if infinite-temperature autocorrelation functions in open chains show anomalous behaviors as a function of time for this model. A motivation to do so is provided by the observation of infinite (long) coherence times for boundary spins for the TFIM without (with) integrability-breaking perturbations due to the presence of a strong zero mode (an almost strong zero mode) that commutes (almost commutes) with the Hamiltonian [29–33]. While the TFIM can be mapped to free fermions by the standard Jordan-Wigner transformations, the perturbed TFIM has additional four-fermion interactions. It is not known if the three-spin model has analogous (almost) strong zero modes. A study of the autocorrelators near the ends of a long system may possibly shed light on this.

The plan of this paper is as follows. In Sec. II, we present the Hamiltonian of the model with three-spin interactions and its symmetries. We find that the model has a $Z_2 \times Z_2$ symmetry which leads to some degeneracies in the energy spectrum of a system with PBC. In Sec. III, we discuss the duality of the model. While the duality is easy to show for an infinite-sized system, we discover that the existence of a duality is a subtle issue for finite-sized systems with PBC. In Sec. IV, we make a detailed study of the criticality properties of the model at the self-dual point given by $h = 1$, using ED for systems with PBC. Finite-size scaling is used to first confirm that there is a critical point at $h = 1$ and then to compute the dynamical critical exponent z, the order parameter exponent β, the magnetic susceptibility exponent γ, and the correlation length exponent ν. We find that $z = 1$ suggesting that the low-energy sector of the model at $h = 1$ has conformal invariance. We then determine the central charge c and find that it is close to 1. Next, we observe that although the values of β, γ and ν for the two-spin and three-spin models are different from each other, the ratios β/ν and γ/ν are the same in the two models. This suggests that there is a weak universality [34] and the three-spin model lies on the Ashkin-Teller (AT) line, just like two copies of the TFIM and the four-state Potts model. Using the numerically computed value of ν for the three-spin model, we estimate the location of this model on the AT line of critical points. We then perform a more careful analysis of the nature of the critical point using the density-matrix renormalization group (DMRG) method that allows us to access much larger system sizes, but with open boundary conditions, compared to the ED method. We find evidence for important additive and multiplicative logarithmic corrections in the critical regime which match those expected at the critical point of the four-state Potts model. Incorporating these logarithmic corrections as well as comparing with the corresponding quantities for the quantum AT model, the data for larger chains suggests that the self-dual point for the three-spin model may be in the same universality as the four-state Potts model.

In Sec. V, we study the energy level spacing statistics to determine if the three-spin model is integrable. We find that the level spacing statistics has the form of the Gaussian orthogonal ensemble, and hence the model is nonintegrable. Next, we find that the model has an exponentially large number of mid-spectrum zero-energy eigenstates. Further, we find that the zero-energy eigenstates are of two types which we call type I and type II. The type-I states are simultaneous zero-energy eigenstates of the two parts of the Hamiltonian (the three-spin interaction and the transverse field) and consequently stay unchanged as a function of h, thus violating the ETH. Hence they qualify as quantum many-body scars. We give exact expressions for a subset of these type-I states in terms of *emergent* singlets and triplets which shows that their number increases at least linearly with system size. In Sec. VI, we study the infinite-temperature autocorrelation function at sites close to one end of a large system and in the bulk with open boundary conditions; the purpose of this study is to understand if there are any states which can be interpreted as the end modes of a semi-infinite system. We find that far from the critical point, at either $h \ll 1$ or $h \gg 1$, some of the autocorrelators show an anomalous behavior in that they oscillate and also decay very slowly with time. We provide a qualitative understanding of the oscillatory behavior using perturbation theory. For values of h close to the critical point, the infinite-temperature autocorrelators decay quickly to zero except for a particular autocorrelator at the end site. In Sec. VII, we summarize our main results and point out some directions for future research.

In brief, we have studied several aspects of a spin-1/2 model with three-spin Ising interactions and placed in a transverse field. The features studied include the duality and other symmetries of the model and its energy spectrum, the continuous phase transition and its critical exponents at the self-dual point $h = 1$, a weak universality of the critical exponents indicating that the model lies on the Ashkin-Teller line, in fact, possibly exhibiting four-state Potts universality, an analysis of the of energy level spacing indicating the nonintegrability of the model, the presence of an exponentially large number of states with exactly zero energy, the existence of a subset of the zero energy states which are many-body scar states (along with an exact analytical expression for some of these scar states), and infinite-temperature autocorrelation functions near the ends of a finite-sized system which show anomalous relaxation with time.

We would like to mention here that several other one-dimensional models with multispin interactions have been studied over the years, and they show a wide variety of unusual features [35–37]. Our work makes a contribution to this interesting area of research.

II. THE MODEL AND ITS SYMMETRIES

The Hamiltonian of the three-spin model is given by [7–12]

$$H_3 = -\sum_{j=1}^{L} \left[\sigma_j^z \sigma_{j+1}^z \sigma_{j+2}^z + h\, \sigma_j^x\right], \tag{2}$$

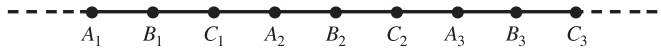

FIG. 1. The lattice for the Hamiltonian H_3 with three sublattices A, B, and C are shown here. The symmetry operators are defined with respect to these sublattices in Eq. (5).

where σ_j^a (where $a = x, y, z$) denotes the Pauli matrices at site j, and we assume PBC so that $\sigma_{L+1}^a = \sigma_1^a$ and $\sigma_{L+2}^a = \sigma_2^a$.

There are three operators D_1, D_2, and D_3 which commute with the Hamiltonian H_3 in Eq. (2). If the system size L is a multiple of 3, we can divide the lattice into three sublattices A, B and C as shown in Fig. 1. The three operators for this system are then defined

$$\begin{aligned} D_1 &= \Pi_{j=1}^{L/3} \sigma_x^{A_j} \sigma_x^{B_j}, \\ D_2 &= \Pi_{j=1}^{L/3} \sigma_x^{B_j} \sigma_x^{C_j}, \\ D_3 &= \Pi_{j=1}^{L/3} \sigma_x^{C_j} \sigma_x^{A_j}. \end{aligned} \tag{3}$$

These satisfy the constraint $D_1 D_2 D_3 = I$. Thus we have four decoupled sectors corresponding to the different allowed values of these operators; $(D_1, D_2, D_3) = (1, 1, 1), (1, -1, -1), (-1, 1, -1)$ and $(-1, -1, 1)$. Thus this model has a $Z_2 \times Z_2$ symmetry. All the four sectors have equal number of states. We also notice that the operator $C = \Pi_{j=1}^{L} \sigma_y$ anticommutes with the Hamiltonian. Hence for every state $|\psi\rangle$ with energy E, there is a state $C|\psi\rangle$ with energy $-E$ due to which the spectrum of this model has a $E \to -E$ symmetry.

With PBC the system also has translation symmetry. If the translation operator is given by U, then we can see from Eq. (3), that

$$\begin{aligned} U D_1 U^{-1} &= D_2, \\ U D_2 U^{-1} &= D_3, \\ U D_3 U^{-1} &= D_1. \end{aligned} \tag{4}$$

We can further see that a combination of these three operators $D' = D_1 + \omega D_2 + \omega^2 D_3$ where ω is the cube root of unity, transforms into $e^{-i2\pi/3}(D_1 + \omega D_2 + \omega^2 D_3)$ upon translation by one site. This is because $U(D_1 + \omega D_2 + \omega^2 D_3)U^{-1} = \omega^2(D_1 + \omega D_2 + \omega^2 D_3)$. This means that for a state $|\psi_k\rangle$ with momentum k, that is, $U|\psi_k\rangle = e^{ik}|\psi_k\rangle$, we have a state $(D_1 + \omega D_2 + \omega^2 D_3)|\psi_k\rangle = e^{-i2\pi/3} e^{ik}|\psi_k\rangle = |\psi_{k-2\pi/3}\rangle$ with momentum $k - 2\pi/3$. Similarly, we have a state $(D_1 + \omega^{-1} D_2 + \omega^{-2} D_3)|\psi_k\rangle$ for which the momentum is $k + 2\pi/3$. Since the D operators commute with the Hamiltonian, the states $|\psi_k\rangle$, $|\psi_{k-2\pi/3}\rangle$ and $|\psi_{k+2\pi/3}\rangle$ are degenerate. However in the sector $(D_1, D_2, D_3) = (1, 1, 1)$, the operators $D_1 + \omega D_2 + \omega^2 D_3$ and $D_1 + \omega^2 D_2 + \omega D_3$ give zero when they act on a state $|\psi_k\rangle$. Therefore the states belonging to this sector do not have a degenerate partner. Thus in the entire spectrum, three-fourths of the states have an exact threefold degeneracy whereas the other one-fourth belonging to the sector (1,1,1) has no degeneracy. We also have a parity symmetry in this system. For an even system size, we can define parity as a mirror reflection about the middle bond. The parity operator then takes the operator $D_1 \to D_2$ and $D_2 \to D_1$ and keeps D_3 unchanged. Thus, for a system with open boundary conditions which breaks translation symmetry, we can still have degeneracies coming from parity symmetry. These come from the states in sectors $(D_1, D_2, D_3) = (1, -1, -1)$ and $(-1, 1, -1)$ as they go to a different sector under parity.

III. DUALITY OF THE MODEL

Just like the TFIM, the three-spin model also exhibits duality on an *infinitely large* system. We show this by starting from the original lattice with sites labeled by an integer j which goes from $-\infty$ to $+\infty$. Then the sites of dual lattice also lie at j. (This is in contrast to the TFIM where the sites of the dual lattice lie at $j + 1/2$.) The transformation of the Pauli matrices going from the original lattice σ_j^a to the dual lattice $\tilde{\sigma}_j^a$ is given by

$$\begin{aligned} \tilde{\sigma}_{j+1}^x &= \sigma_j^z \sigma_{j+1}^z \sigma_{j+2}^z, \\ \tilde{\sigma}_{j-1}^z \tilde{\sigma}_j^z \tilde{\sigma}_{j+1}^z &= \sigma_j^x. \end{aligned} \tag{5}$$

The Hamiltonian on the dual lattice then takes the form

$$\tilde{H}_3 = -\sum_{j=-\infty}^{\infty} \left[\tilde{\sigma}_{j+1}^x + h\, \tilde{\sigma}_{j-1}^z \tilde{\sigma}_j^z \tilde{\sigma}_{j+1}^z\right]. \tag{6}$$

Thus going from H_3 to $\tilde{H}_3$, the transverse field h gets mapped to $1/h$. The self-dual point lies at $h = 1/h$. Hence, if H_3 (or $\tilde{H}_3$) has a phase transition it must occur at $|h| = 1$.

We will now examine if duality also holds for a *finite* system with PBC as described in Eq. (2). Clearly, we would like both the original and dual lattices to have the same number of sites, L, and the number of states should be 2^L in both cases. The latter can only happen if the Pauli operators are independent operators on different sites on both the lattices. The first equation in Eq. (9) and the fact that $(\sigma_j^z)^2 = 1$ for all j imply that

$$\begin{aligned} \tilde{\sigma}_1^x \tilde{\sigma}_2^x \tilde{\sigma}_4^x \tilde{\sigma}_5^x \cdots \tilde{\sigma}_{L-2}^x \tilde{\sigma}_{L-1}^x = I, \\ \text{and} \quad \tilde{\sigma}_2^x \tilde{\sigma}_3^x \tilde{\sigma}_5^x \tilde{\sigma}_6^x \cdots \tilde{\sigma}_{L-1}^x \tilde{\sigma}_L^x = I \end{aligned} \tag{7}$$

if L is a multiple of 3. Hence there are two constraints on the $\tilde{\sigma}_j^x$ operators, implying that the eigenvalues of the operators cannot take all possible values independently of each other. To put it differently, the two constraints mean that the number of states in the dual system is 2^{L-2} rather than 2^L. We reach a similar conclusion for the original system by using the second equation in Eq. (9). We therefore conclude that duality does not hold for a finite system with PBC if L is a multiple of 3. It turns out that duality does hold if L is *not* a multiple of 3 as the Pauli operators do not satisfy any constraints on either the original lattice or the dual lattice in that case. (Note, however, that the operators D_j defined in Sec. II do not exist if L is not a multiple of 3). Next, duality implies that there must be a unitary operator U_D which relates the states of the original and dual lattices. Let us write the Hamiltonian in Eq. (2) in the form

$$\begin{aligned} H_3 &= -Z - hX, \\ \text{where } Z &= \sum_{j=1}^{L} \sigma_j^z \sigma_{j+1}^z \sigma_{j+2}^z, \\ X &= \sum_{j=1}^{L} \sigma_j^x, \end{aligned} \tag{8}$$

and similarly

$$\tilde{H}_3 = -\tilde{X} - h\tilde{Z}. \tag{9}$$

Then there must be a unitary operator U_D such that $U_D X U_D^{-1} = \tilde{Z}$ and $U_D Z U_D^{-1} = \tilde{X}$. This means that at the self-dual point $h = 1$, if $|\psi_n\rangle$ is an eigenstate of H_3 with eigenvalue E_n, and $|\tilde{\psi}_n\rangle = U_D|\psi\rangle$ is an eigenstate of $\tilde{H}_3$ with the same eigenvalue, we must have

$$\langle\psi_n|X|\psi_n\rangle = \langle\tilde{\psi}_n|\tilde{Z}|\tilde{\psi}_n\rangle = \langle\psi_n|Z|\psi_n\rangle, \tag{10}$$

where the equality $\langle\tilde{\psi}_n|\tilde{Z}|\tilde{\psi}_n\rangle = \langle\psi_n|Z|\psi_n\rangle$ is a consequence of self-duality. Since $\langle\psi_n|(-X - Z)|\psi_n\rangle = E_n$, Eq. (10) implies that

$$\langle\psi_n|X|\psi_n\rangle = -\frac{E_n}{2}. \tag{11}$$

at $h = 1$. A test of this relation will be discussed in Appendix B.

Before ending this section, we note that it is not useful to perform a Jordan-Wigner transformation from spin-1/2's to spinless fermions for this model because there are three-spin terms in the Hamiltonian. The Jordan-Wigner transformation maps σ_j^x to the occupation number $c_j^\dagger c_j$ of fermions at site j, and σ_j^z to $c_j + c_j^\dagger$ times a string of σ_n^x operators running from $n = -\infty$ to $j - 1$ (for an infinitely large system). The presence of the three-spin term $\sigma_j^z \sigma_{j+1}^z \sigma_{j+2}^z$ in the Hamiltonian implies there will be an infinitely long string of σ_n^x operators left over which does not cancel with anything. Thus this model cannot be solved by fermionizing since the fermionic Hamiltonian will have highly nonlocal terms. We will henceforth analyze the model numerically. In the next section, we will carry out ED calculations to confirm the location of the critical point of the quantum phase transition and to extract the critical exponents.

IV. QUANTUM CRITICALITY OF THE MODEL

We will now study the three-spin model numerically to understand the nature of the phase transition at $h = 1$ and the critical properties. We will use ED to obtain the ground state and low-lying excitations and then compute various thermodynamic quantities like the magnetization and magnetic susceptibility to study the criticality.

A. Energy levels

We use ED to compute the first few energy levels for the Hamiltonian in Eq. (2). The first three excited energy levels with respect to the ground state energy are plotted in Fig. 2. We first notice that the phase transition happens close to $|h| = 1$. In the region $|h| > 1$, the system is gapped with a finite difference between the ground state and the first excited energy. The first three excited states are exactly degenerate due to the symmetries D_1, D_2, D_3 of the model (see Sec. II) with eigenvalues $(D_1, D_2, D_3) = (1, -1, -1), (-1, 1, -1)$, and $(-1, -1, 1)$. The ground state is unique and belongs to the sector $(D_1, D_2, D_3) = (1, 1, 1)$. In the region $|h| < 1$, the ground state becomes degenerate with the threefold degenerate states as the system size approaches infinity. For finite-sized systems, there is a small gap in the region $|h| < 1$. The gap varies with h and falls off exponentially with the system size; for $h = 0.4$ and $L = 15$, the gap is of the order of 10^{-4}.

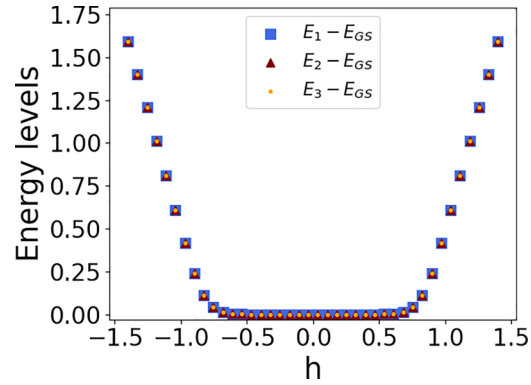

FIG. 2. First three energy levels as measured from the ground state energy plotted as a function of the transverse field h for $L = 15$. We see some degeneracies which arise from the $Z_2 \times Z_2$ symmetry.

B. Finite-size scaling

To understand the nature of the phase transition in this model in comparison to the TFIM which has two-spin interactions, we look at the behaviors of different quantities close to the critical point. Close to the critical point, any singular quantity, Θ, will have an asymptotic behavior of the form [38]

$$\Theta \sim |h - h_c|^{-\theta}, \tag{12}$$

where θ is the critical exponent of the quantity Θ. In addition, continuous phase transitions have a diverging correlation length scale ξ which diverges close to the critical point as $\xi \sim |h - h_c|^{-\nu}$, where ν is the critical exponent corresponding to the correlation length. This implies that $\Theta \sim \xi^{\theta/\nu}$. At the critical point, the correlation length diverges. However for finite system sizes, we are limited by the system size L. Hence, when the correlation length exceeds the system size, the quantity will vary with L depending on the ratio L/ξ, and the above relation gets modified to

$$\Theta \sim \xi^{\theta/\nu} \Theta_0(L/\xi), \tag{13}$$

where $\Theta_0(L/\xi)$ is a scaling function with

$$\Theta_0(L/\xi) = \begin{cases} \text{constant} & \text{for } L \gg \xi \\ (L/\xi)^{\theta/\nu} & \text{for } L \ll \xi \end{cases}.$$

Thus at the critical point when $\xi \gg L$, we find that Θ scales as [38]

$$\Theta|_{h_c} \sim L^{\theta/\nu}. \tag{14}$$

By evaluating Θ for different system sizes we can calculate the critical exponent θ/ν once we know the exact location of the critical point h_c.

C. Numerical determination of critical point

The ground state fidelity is the one of the preliminary ways to detect a quantum phase transition. The fidelity is defined as $\mathcal{F}(h, \delta h) = |\langle\psi_0(h - \delta h/2) \mid \psi_0(h + \delta h/2)\rangle|$, where $\psi_0(h \pm \delta h/2)$ is the ground state of the Hamiltonian with parameter $h \pm \delta h/2$, and δh is a small but fixed number. The

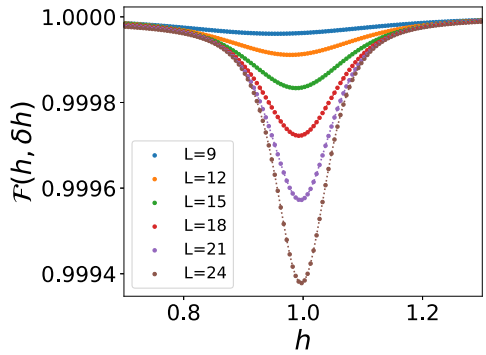

FIG. 3. Fidelity as a function of the transverse field h (for a fixed $\delta h = 0.005$) is plotted for different system sizes $L = 9,\ 12,\ 15,\ 18,\ 21$, and 24. There is a dip in the fidelity close to the expected critical point $h = 1$.

fidelity is expected to show a pronounced deviation from unity in the neighborhood of a phase transition.

In Fig. 3, we show the variation of the fidelity $\mathcal{F}(h, \delta h)$ as a function of the transverse field h for different system sizes $L = 9,\ 12,\ 15,\ 18,\ 21,$ and 24 for a fixed $\delta h = 0.005$. We see a dip close to $h = 1$ for all system sizes confirming that a phase transition occurs at this point. As the system size increases, the magnitude of the dip increases and the location of the dip approaches the predicted value $h = 1$. For the largest system size here $L = 24$, we find that the minimum occurs at $h_c = 0.9960$. We also note that the location of the minimum, $h_c(L)$, obtained from the fidelity scales as $h_c(L) = 1 + aL^{-2/\nu}$, while the value of the fidelity susceptibility $\chi_F(h_c = 1) = -\partial^2\mathcal{F}(h_c, \delta h)/\partial^2(\delta h)|_{\delta h \to 0}$ at $h_c = 1$ scales as $bL^{2/\nu}$, where a, b are constants and ν is the correlation length exponent yielding $\nu \approx 0.71$ (see Sec. IV H for further discussion).

D. Dynamical critical exponent z

The smallest energy gap in the system at finite sizes (Fig. 2) can be used to estimate the dynamical critical exponent z. As we approach the critical point, the energy difference between the first excited state and the ground state, Δ, behaves as

$$\Delta \sim |h - h_c|^{z\nu}. \tag{15}$$

Given the exponent $z\nu$, Eqs. (12) and (14) imply that

$$\Delta|_{h_c} \sim L^{-z}. \tag{16}$$

We evaluate Δ by performing ED for various system sizes $L = 12,\ 15,\ 21,\ 24,$ and 27 in the neighborhood of the critical point. Figure 4(a) shows the variation of Δ with h for different system sizes. At $h = h_c$ we plot a log-log graph of $\Delta|_{h_c}$ versus L [inset of Fig. 4(a)], and fit it linearly to obtain the slope. We find that $z = 1.0267 \pm 0.0014$ indicating that $z = 1$ at criticality.

E. Calculation of central charge c

Since the critical exponent $z = 1$ for this model, the low-lying excitations at the critical point have a linear dispersion making the system Lorentz invariant with some velocity v which will be discussed below. Thus the model can be described by a $1 + 1$-dimensional conformal field theory characterized by a central charge c [6]. In such a theory, the von Neumann entanglement entropy of the system can be used to extract the central charge c. If the system is divided into two subsystems A and B, the von Neumann entanglement entropy between the two systems is given by

$$S_A = -\mathrm{Tr}_A(\rho_A \ln \rho_A), \tag{17}$$

where ρ_A is the reduced density matrix of the subsystem A obtained by tracing out the states in B from the density matrix of the ground state: $\rho_A = Tr_B\, |\psi_{GS}\rangle\, \langle\psi_{GS}|$. For a finite system size L with PBC, if we divide the system into two subsystems with sizes l and $L - l$, the von Neumann entanglement entropy for the subsystem l is found to be [39]

$$S(l) = \frac{c}{3} \ln[g(l)] + c', \tag{18}$$

where $g(l) = (L/\pi)\sin(\pi l/L)$, and c' is a constant. For our model, we take $L = 27$ and calculate $S(l)$ for different

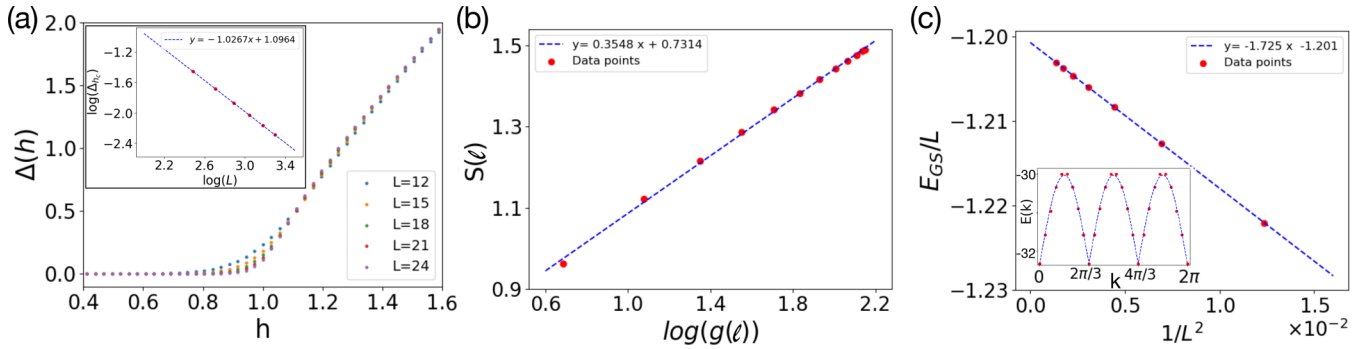

FIG. 4. (a) Plot of the smallest gap, Δ, as a function of h for different system sizes. The inset shows a log-log plot of $\Delta|_{h_c}$ fitting which to a straight line gives the dynamical exponent $z = 1.0267 \pm 0.0014$. (b) Plot of the ground state entanglement entropy versus the logarithm of $g(l) = (L/\pi)\sin(l\pi/L)$, where l is the size of one of the subsystems, and $L = 27$ at the critical coupling $h_c = 1$. The slope of the graph is $c/3$ which gives $c = 1.0644$. (c) From Eq. (19), the variation of the ground state energy with the system size L at $h_c = 1$ gives an estimate for c, namely, the slope of E_{GS}/L versus $1/L^2$ has a slope equal to $-\pi v c/(6L)$. For $L = 27$, we find that $c = 0.9585$. The inset shows the velocity estimate of the gapless excitations which is calculated by fitting the function $E(k) = a\sin(bk) + d$. For $L = 27$, we find $a = 2.2893$ and $b = 1.5012$ respectively giving the velocity $v = ab = 3.4367$.

subsystems l, plot $S(l)$ [Fig. 4(b)] as a function of $\ln[g(l)]$, and fit it linearly. The central charge c is three times the slope obtained from this fit which gives $c = 1.0644 \pm 0.0072$.

We can use another method to calculate c. The ground state energy of a finite-sized system is found to show the following dependence on the system size L [39],

$$E_{GS} = \alpha L - \frac{\pi v c}{6L}, \tag{19}$$

where α is a nonuniversal constant equal to the ground state energy per site in the thermodynamic limit [40], v is the velocity of the gapless excitations at the critical point which can be obtained from the dispersion, and c is the central charge. We first calculate the velocity by plotting the dispersion for $L = 27$ as shown in the inset of Fig. 4(c). As discussed earlier, the dispersion varies periodically with the momentum with a period equal to $2\pi/3$. Fitting the inset in Fig. 4(c) with a function of the form $E = a\sin(bk) + d$, where $a = 2.2893 \pm 0.0134$ and $b = 1.5012 \pm 0.0015$ respectively (the value of b is consistent with a period of $2\pi/3$. Thus the velocity in the linear region near $k = 0$ is $v = ab = 3.4367 \pm 0.0236$. The slope of E_{GS}/L versus $1/L^2$ shown in Fig. 4(c) gives a slope equal to $-\pi v c/(6L)$. Putting all this together, we get the value of c for this model to be $c = 0.9585 \pm 0.0015$. Thus both the methods give an estimate of c which is close to 1. A value of $c = 1$ suggests the possibility of a marginal operator at the critical point [41] of the three-spin model, and hence weak universality. To investigate this further, we proceed to compute the other critical exponents of this system: β related to the order parameter, γ to the magnetic susceptibility, and ν to the correlation length.

F. Order parameter exponent β

We now study the order parameter in this model. Given the three-spin form of the interaction, we define a symmetric order parameter as follows. As described earlier, the lattice has three sublattices A, B, and C. We define three quantities

$$m_A = \frac{3}{L}\sum_{n=1}^{L/3}\sigma^z_{3n-2},$$
$$m_B = \frac{3}{L}\sum_{n=1}^{L/3}\sigma^z_{3n-1},$$
$$m_C = \frac{3}{L}\sum_{n=1}^{L/3}\sigma^z_{3n}, \tag{20}$$

and a combined order parameter

$$m = \sqrt{\langle m_A^2\rangle + \langle m_B^2\rangle + \langle m_C^2\rangle}. \tag{21}$$

For numerical clarity, it would be worthwhile to note here that for finite-size systems, the ground state expectation values $\langle m_a\rangle$ are equal to zero for $a = A, B, C$ even for $h < h_c$. This is due to the fact that the ground state is fourfold degenerate (in the infinite size limit), and the ground state obtained from ED is a linear combination of these four states making the expectation values exactly equal to zero. To bypass this problem we have first evaluated $\langle m_a^2\rangle$ and then taken the square root of the squares. The behavior of m for our model as a function of transverse field h is shown in Fig. 5(a). It begins to drop to zero as we approach h_c. Close to the critical point, we have

$$m \sim |h - h_c|^{\beta}. \tag{22}$$

From the finite-size scaling of magnetization, we have

$$\mathcal{M}_z \sim L^{-\beta/\nu}, \tag{23}$$

where $\mathcal{M}_z = m|_{h_c}$. The log-log graph for $\mathcal{M}_z$ versus L is shown in the inset of Fig. 5(a); from this, we find that $\beta/\nu = 0.1291 \pm 0.0018$. This ratio is close to the value of $\beta/\nu = 1/8$ found for the TFIM (two-spin model) where it is analytically known that $\beta = 1/8 = 0.125$ and $\nu = 1$.

G. Magnetic susceptibility exponent γ

We now compute the magnetic susceptibility χ. For this calculation, we add a longitudinal field to the system so that the Hamiltonian becomes

$$H = -\sum_{j=1}^{L}\left[\sigma_j^z\sigma_{j+1}^z\sigma_{j+2}^z + h\sigma_j^x + h_z\sigma_j^z\right], \tag{24}$$

where h_z is the longitudinal field in the system.

The magnetic susceptibility is defined as [42]

$$\chi = \left.\frac{\partial\langle M_{h_c}\rangle}{\partial h_z}\right|_{h_z\to 0}, \tag{25}$$

where $\langle M_{h_c}\rangle$ is computed as follows. We first define $M = \frac{1}{L}\sum_{i=1}^{L}\sigma_i^z$ and evaluate its expectation value in the ground state as a function of the transverse and longitudinal fields h_z and h. It will be nonzero due to the presence of the longitudinal field. At the critical point $h_c = 1$ we take the derivative of M_{h_c} with respect to h_z and find its value in the limit $h_z \to 0$. The magnetic susceptibility as a function of the transverse field h is shown in Fig. 5(b).

For different system sizes at the critical point we have the quantity $\chi_0 = \chi|_{h_c}$ which, from finite-size scaling, behaves as

$$\chi_0 \sim L^{\gamma/\nu}, \tag{26}$$

where γ is the exponent corresponding to susceptibility. This is estimated by plotting a log-log graph of χ_0 versus L as shown in the inset of Fig. 5(b). The ratio of the exponents γ/ν comes out to be 1.7976 ± 0.0034 for this model, which is close to the value of $\gamma/\nu = 7/4$ known for the TFIM where $\gamma = 7/4 = 1.75$ and $\nu = 1$.

H. Correlation length exponent ν

To evaluate the correlation length exponent, we return to Eq. (13). Reorganizing that equation using the relation $\tilde{\Theta}(y) = y^{\theta}\Theta_0(y^{\nu})$, we get

$$\Theta L^{-\theta/\nu} \sim \tilde{\Theta}(L^{1/\nu}|h - h_c|). \tag{27}$$

By choosing the thermodynamic quantity Θ to be the smallest energy gap Δ and by fixing the corresponding exponent z to be 1 as obtained earlier, we look at the derivative of Eq. (27) with respect to h. At the critical point, we therefore have

$$\left.\frac{d(\Delta L^z)}{dh}\right|_{h_c} \sim L^{1/\nu}. \tag{28}$$

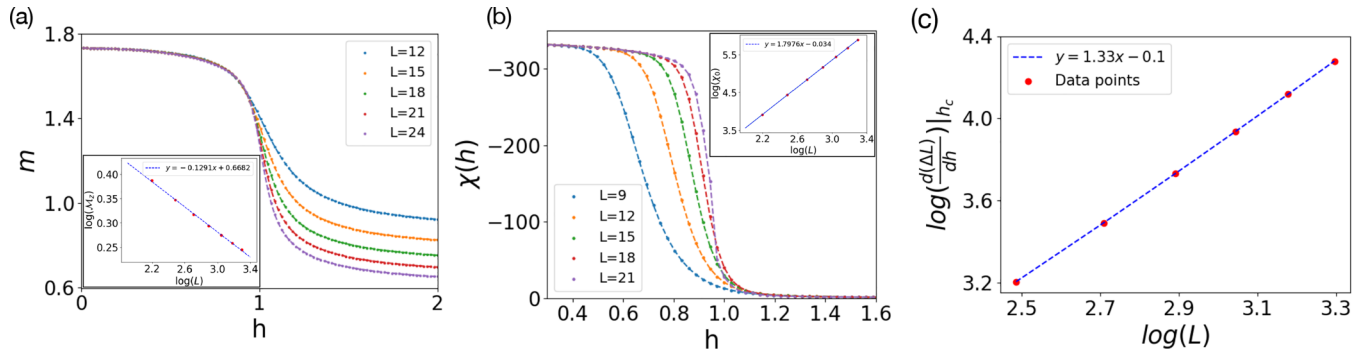

FIG. 5. (a) Plot of the order parameter defined in Eq. (21) versus h for different system sizes. We see that it has a finite value for $h < 1$ and falls off as $h > 1$. The log-log plot of this quantity at the critical point with maximum system size $L = 27$ gives a slope of β/ν close to 0.129. (b) Plot of the magnetic susceptibility for this model as a function of h. At the critical point, it scales with the system size with an exponent γ. From the log-log plot shown in the inset, we find that $\gamma/\nu = 1.7976$. (c) A log-log plot of $d(\Delta(h)L)/dh|_{h_c}$ at the critical point vs L. The slope gives us the inverse of the exponent of correlation length ν. From this data fitting, we obtain the value of ν to be 0.7538.

In Fig. 5(c), we plot the logarithm of $\frac{d(\Delta L^z)}{dh}|_{h_c}$ versus the logarithm of the system sizes with $L = 12$, 15, 18, 24, and 27. From the slope of the data fitting, we find the value of $\nu = 0.7538$. From this analysis, we see that the critical point of the three-spin model is different from the TFIM (where $\nu = 1$) even though the values of β/ν and γ/ν seem to be identical.

I. Comparison with transverse field Ising model, hyperscaling, and quantum Ashkin-Teller model

We have repeated the numerical analysis for the TFIM (two-spin Ising model) using ED for system sizes $L =$ 8, 10, 12, 14, 16, 18, 20, and 22. In that case our calculations give $z = 1.0026$, $c \approx 0.50$, $\beta/\nu = 0.1337$, and $\gamma/\nu = 1.7936$. For the three-spin model we found above that $z = 1.02$, $\beta/\nu = 0.129$, and $\gamma/\nu = 1.798$ with the data from system sizes $L = 9$, 12, 15, 18, 21, 24, and 27. We can see that the values of the ratios of critical exponents β/ν and γ/ν are very close to each other for the two models. However the correlation length critical exponent ν is 1 for the two-spin model (TFIM) and close to 0.75 for the three-spin model. Since all the exponents and the central charge value conform with the theoretical values from analytical and numerical calculations for the two-spin Ising model [38,43], we expect that the exponents obtained by the same methods for the three-spin model are also reliable. The estimated values for the two models are tabulated and compared in Table I. Furthermore, we check for the validity of the hyper-scaling relation for our model. The hyperscaling relation is given by [38]

$$2\beta + \gamma = \nu(d + z), \tag{29}$$

where d is the space dimensionality of the system ($d = 1$ in our case). Since d, z, β/ν, and γ/ν are the same for the two-spin and three-spin models, our model also satisfies the hyperscaling relation.

Since the central charge $c = 1$ for the three-spin model and the ratios of the critical exponents β/ν and γ/ν are essentially identical to those of the TFIM, this strongly suggests that the critical behavior of the three-spin model belongs to the class of $1 + 1$-dimensional models with $z = 1$ and $c = 1$ described by the AT model [44]. The AT model constructed on a lattice has two spin $s = 1/2$ freedom on each site denoted by σ and τ. These operators are coupled by a parameter λ. The Hamiltonian for the quantum AT model is given by [45]

$$H_{AT} = -\sum_{j=1}^{L} \left(\sigma_j^z \sigma_{j+1}^z + \tau_j^z \tau_{j+1}^z + \lambda \sigma_j^z \sigma_{j+1}^z \tau_j^z \tau_{j+1}^z\right)$$
$$-h \sum_{j=1}^{L} \left(\sigma_j^x + \tau_j^x + \lambda \sigma_j^x \tau_j^x\right). \tag{30}$$

For any value of λ and h, this model has a $Z_2 \times Z_2$ symmetry, where the two Z_2's are given by ($\sigma_j^z \to -\sigma_j^z$, $\sigma_j^x \to \sigma_j^x$) and ($\tau_j^z \to -\tau_j^z$, $\tau_j^x \to \tau_j^x$), respectively.

At the critical point $h = 1$, the model in Eq. (30) is known to exhibit weak universality, namely, the ratios of the exponents $\beta/\nu = 1/8$ and $\gamma/\nu = 7/4$ are independent of λ but the values of the exponents individually depend on λ. One limit of $\lambda = 0$ reduces the AT model to two decoupled TFIM thus giving $c = 1$. For this case, we know that $\nu = 1$. In the other limit of $\lambda = 1$, we get the four-state Potts model [46], with the critical exponent $\nu = 2/3$. We thus see that our three-spin model H_3 also appears to show this weak universality since $c = 1$, and β/ν and γ/ν are close to $1/8$ and $7/4$. However, ν is different from the TFIM. Since the value of $\nu = 0.7538$

TABLE I. Numerical estimates of the critical exponents and the central charge for the three-spin and two-spin Ising models in a transverse field. Here EE stands for entanglement entropy. The error bars shown are obtained from the fitting procedures as discussed in the text.

Exponent	Method used	Three-spin	Two-spin
z	Δ scaling with L at h_c	1.0267 (14)	1.0026 (3)
β	m scaling with L at h_c	0.0973 (14)	0.1337 (64)
γ	χ scaling with L at h_c	1.3550 (84)	1.7936 (20)
ν	$\frac{d}{dh}(\Delta L)$ scaling with L at h_c	0.7538 (45)	1.0335 (42)
c	EE Scaling at h_c	1.0644 (72)	0.5096 (13)
	Energy scaling at h_c	0.9585 (15)	0.5034 (68)

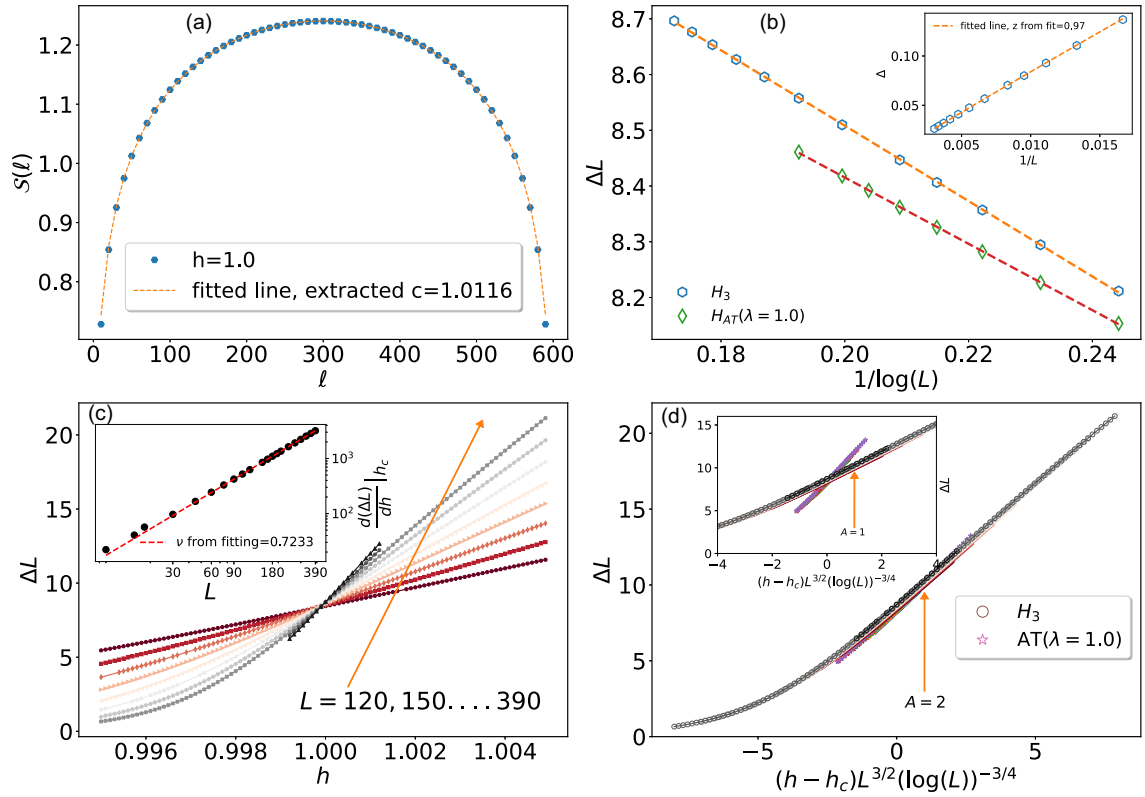

FIG. 6. (a) Behavior of the entanglement entropy $\mathcal{S}(\ell)$ as a function of the subsystem size ℓ in the ground state of the three-spin model at the critical point $h_c = 1$ for $L = 600$. (b) Behavior of ΔL as a function of system size for both the three-spin model and the AT model at $\lambda = 1$ is consistent with the form shown in Eq. (31). The inset shows the result of fitting the corresponding data for the three-spin model to the form $\Delta|_{h_c} \sim L^{-z}$. (c) Plot of ΔL versus h in the vicinity of $h_c = 1$ for various L shown for the three-spin model. The inset shows the determination of the exponent ν using $\frac{d(\Delta L)}{dh}|_{h_c} \sim L^{1/\nu}$. (d) ΔL in the neighborhood of h_c, both for the three-spin model and the AT model at $\lambda = 1$, can be collapsed to the same universal curve by assuming the scaling form shown in Eq. (32) and choosing the metric factor $A = 1$ in the former case and $A \approx 2$ in the latter case. The inset shows the scaling collapse assuming Eq. (32) without adjusting for the different metric factors in the two different models.

for the three-spin model, results from ED suggest that it must lie somewhere in between two copies of the TFIM and the four-state Potts model. To find the value of λ for which the three-spin model would get mapped to the AT model, we would have to study the AT model as a function of λ. However since the number of degrees of freedom are doubled, we can go only up to system sizes $L = 13$ using ED, and thus cannot rely on those numerical results. We note that the value of $\nu \approx 0.75$ for the three-spin model is consistent with the values obtained earlier by finite-size scaling for system sizes up to $L = 18$ [9–11] and by series expansions [12].

J. DMRG results

We now present the results extracted from studies using the density-matrix renormalization group (DMRG) method [47,48] for the three-spin model with open boundary conditions (OBC). The primary objective of performing the DMRG is to better understand the nature of the critical point at $h_c = 1$. We implement DMRG using the ITENSOR (JULIA) library [49]. The reasons for using OBC while performing DMRG studies are twofold: (i) the traditional DMRG algorithm (and the one used by the ITENSOR library) is based on optimization of open matrix product states [50], and (ii) even though one can try in a straightforward manner to implement DMRG with PBC simply by including a "long bond" directly connecting the two ends of the systems, such a naive approach suffers from serious drawbacks. In particular, if DMRG with OBC achieves a certain accuracy while keeping χ states (where χ denotes the bond dimension), then to reach the same accuracy with PBC, one needs to keep approximately χ^2 states [50]. This drawback of the DMRG method with PBC makes it rather costly and therefore impractical. We note that although there are certain proposals for efficient DMRG studies with PBC [51], such proposals are yet to be well tested for critical systems to the best of our knowledge.

Using DMRG, we first compute the entanglement entropy $\mathcal{S}(\ell)$ as a function of the subsystem size ℓ in the ground state of the three-spin model at the critical point $h_c = 1$. We extract the central charge c using the well-known relation $\mathcal{S}(\ell) = (c/6)\ln((L/\pi a)\sin(\pi\ell/L)) + c'$ [39] on open chains. As shown in Fig. 6(a), using data for a system size of $L = 600$, we get $c = 1.0116 \pm 0.00071$ (along with $c' = 0.3552 \pm 0.00058$) which provides strong evidence that the $h_c = 1$ critical point is described by a $c = 1$ conformal field theory. Furthermore, we can reliably extract the smallest excitation gap above the ground state, Δ, in the neighborhood of $h_c = 1$ for open chains up to $L \leqslant 390$ which gives us a way

to estimate both z and ν. We also calculate the smallest gap, Δ, in the vicinity of the critical point $h_c = 1$ for the AT model at various values of λ [Eq. (30)] to compare certain universal features at criticality with the three-spin model. Since the local Hilbert space for the AT model is four-dimensional unlike that of the three-spin model, we can only go up to open chains of size $L \leqslant 180$ with our available resources.

As in the ED procedure, we first estimate z using $\Delta|_{h_c} \sim L^{-z}$ [see the discussion around Eq. (16)]. For the three-spin model, using data for $L \in [90, 330]$, we obtain $z \approx 0.97$ which is still reasonably far from the theoretically expected value of $z = 1$ [see the inset of Fig. 6(b)]. In contrast, we obtain $z \approx 0.995$ for the AT model at $\lambda = 0$ (the decoupled Ising limit) even after using smaller system sizes $L \in [75, 180]$. On the other hand, the analysis of Δ for the critical point of the AT model in the vicinity of $\lambda = 1$ again yields $z \approx 0.97$ with the available system sizes. This suggests the presence of slowly decaying corrections in L for $\Delta|_{h_c} L$. It is well-known from the study of the critical properties of the classical two-dimensional four-state Potts model [52,53] that there are important universal additive and multiplicative logarithmic corrections to scaling in many quantities. From the classical-to-quantum correspondence, we expect the same in the one-dimensional quantum version. In fact, one expects a leading additive logarithmic correction of the form [53]

$$\frac{\Delta|_{h_c} L}{|h_c|} = a^* + \frac{b}{\ln(L)} + \cdots, \tag{31}$$

where a^* is a universal number that characterizes the critical point and $\cdots$ refers to terms that decay faster than $1/\ln(L)$. We indeed see from Fig. 6(b) that the smallest gap $\Delta|_{h_c}$ for both the three-spin model and the AT model at $\lambda = 1$ are consistent with this form. We choose to only consider the leading additive logarithmic correction while fitting the data since we only have a limited range of L available to us from DMRG. We estimate $a^* \approx 9.86(9.61)$ from the data for the three-spin model (AT model at $\lambda = 1$) from the available system sizes.

We estimate ν from the DMRG data by using the relation $\frac{d(\Delta L)}{dh}|_{h_c} \sim L^{1/\nu}$ [see the discussion around Eq. (28)] and fitting system sizes in the range of $L \in [90, 390]$ for the three-spin model, from which we extract $\nu = 0.7233 \pm 0.0011$ as shown in the inset of Fig. 6(c). In the main panel of the same figure, we show the behavior of ΔL versus h for different system sizes. We obtain a good scaling collapse (not shown) when ΔL^z (with $z = 1$) is plotted as a function of $(h - h_c)L^{1/\nu}$ (see the discussion around Eq. (27)), with $\nu \approx 0.72$. The significant difference between the numerical values of ν obtained via ED ($\approx$0.75) and DMRG plausibly indicates the strong sensitivity of the system to both finite size effects and the boundary conditions. However, we note that $\frac{d(\Delta L)}{dh}|_{h_c} \sim L^{1/\nu}$ follows from Eq. (27). On the other hand, it is known that there are important multiplicative logarithmic corrections to the scaling form [Eq. (27)] for Δ in the vicinity of the critical point of the two-dimensional classical four-state Potts model. In fact, we expect that

$$\Delta L = \mathcal{F}(A(h - h_c)L^{3/2}(\ln\ L)^{-3/4}) \tag{32}$$

from the behavior of the correlation length near criticality for the two-dimensional classical four-state Potts model [53], where $\mathcal{F}$ denotes a universal function and A denotes a *metric factor* that varies depending on the microscopics of the model. Assuming Eq. (32) gives $\frac{d(\Delta L)}{dh}|_{h_c} \sim L^{3/2}(\ln L)^{-3/4}$ which *mimics* a power law $L^{1/\nu}$ with $\nu \approx 0.72$ given that $L \in [90, 390]$. In fact, the inset of Fig. 6(d) shows that the Δ in the neighborhood of $h_c = 1$ for different L is consistent with this scaling ansatz [Eq. (32)] both for the three-spin model and for the AT model with $\lambda = 1$ (where $L \in [75, 180]$). Note that the inset of Fig. 6(d) requires no fitting parameter. In fact, choosing a metric factor of $A = 1$ for the three-spin model and $A \approx 2$ (by visual inspection) for the AT model at $\lambda = 1$ makes the data for the two different microscopic models fall on the same scale-collapsed curve [Fig. 6(d), main panel], which is strong evidence that the two critical points belong to the same universality class, i.e., four-state Potts criticality.

Since the scaling collapse of the smallest gap, Δ, is consistent with both Eq. (27) with $\nu \approx 0.72$ and Eq. (32), one may ask whether some other quantity can distinguish between the two scenarios. An analytical study using the real-space renormalization group gives a relation between the critical exponents ν and the corresponding λ of the AT model as [54]

$$\nu = \frac{1}{2 - \left(\frac{\pi}{2}\right)[\arccos(-\lambda)]^{-1}}, \tag{33}$$

which gives $\lambda = 0.8267$ for $\nu = 0.7233$ extracted from the behavior of $d(\Delta L)/dh$ at $h_c = 1$ for various values of L assuming a scaling of the form $L^{1/\nu}$(ignoring the statistical error in the fitting procedure). First, fitting $\Delta|_{h_c} \sim L^{-z}$ again yields $z \approx 0.97$ at this λ, similar to the case of the three-spin model and the AT model at $\lambda = 1$. However, even though $\Delta|_{h_c} L$ seems to be consistent with Eq. (31), the extrapolated value of $a^* \approx 7.97$ turns out to be quite different from the corresponding value for the critical point of the three-spin model. Second, it turns out that probing Binder cumulants [55–57], denoted by U_2, constructed from the second and fourth moments of appropriately defined order parameters for the three-spin model, as well as the AT model for both $\lambda = 1$ as well as $\lambda = 0.8267$ helps to clarify the situations.U_2 can be defined such that it equals 1 (0) in the ordered (disordered) phase and attains a nontrivial value U_2^* at the critical point in the thermodynamic limit. For finite systems, U_2 typically displays a monotonic behavior as a function of h, the parameter that drives the quantum phase transition, and thus stays bounded between 0 and 1. On the other hand, U_2 shows a nonmonotonic behavior and in fact develops a negative peak whose location approaches the critical points and whose magnitude diverges polynomially with L as $L \to \infty$ [58,59]. However, from the results for the classical Ashkin-Teller model in two dimensions [60], U_2 is expected to display a *pseudo-first-order behavior* characterized by a nonmonotonic behavior of U_2 in h as well as a negative dip that increases in magnitude with system size, albeit much slower than what is expected from a first-order transition, for the one-dimensional quantum AT model in the neighborhood of $\lambda = 1$ but not sufficiently away from it. Obtaining U_2 from DMRG for finite open chains for the three-spin model, and the AT model at $\lambda = 1$ and $\lambda = 0.8267$ respectively, one sees that while both the three-spin model and the AT model at $\lambda = 1$ shows such pseudo-first-order behavior, U_2 displays a monotonic behavior and is bounded between 0 and 1 for the case of the AT model with $\lambda = 0.8267$

for the available system sizes (see Appendix A for numerical plots and further discussion). We take this as evidence that the three-spin model, in fact, displays four-state Potts criticality and is not in the universality class of an intermediate critical point described by $\lambda \approx 0.83$.

Before ending the discussion of the DMRG results, we point out that we have carefully checked that our results are well converged with respect to the bond dimension. For all the calculations, apart from keeping track of energy convergence, we have also checked that the energy fluctuation in the obtained state $\langle H^2\rangle - \langle H\rangle^2 \sim 10^{-10}$, ensuring that the state obtained at the end of the DMRG calculation is indeed an eigenstate of H. While computing the energy gap, we have explicitly checked that the overlap between ground state and the first excited state obtained via DMRG is of the order 10^{-10}, which ensures their expected orthogonality.

V. PRESENCE OF QUANTUM MANY-BODY SCARS

A. Nonintegrability of the model

We now show that the three-spin model is different from the TFIM in that while the latter model is well-known to be integrable, the former seems to be nonintegrable. A common diagnostic to test integrability is to study the energy level spacing statistics. In this section, we will study that level spacing for H_3 and discover that shows that the model is nonintegrable. If the spectrum of energies is sorted in increasing order so that E_n is the n-th energy level, then we define the level spacing as [61,62]

$$s_n = E_{n+1} - E_n. \tag{34}$$

The distribution of s, called $P(s)$, gives a way of testing the integrability of the system. The system is integrable if $P(s)$ is Poisson-like and is nonintegrable if $P(s)$ has a Wigner-Dyson distribution. However, for many-body systems with a nonconstant density of states, a new quantity proposed by Oganesyan and Huse [63] is more useful and reliable. This quantity $\tilde{r}$ is defined as follows

$$\tilde{r} = \frac{\min(s_n, s_{n-1})}{\max(s_n, s_{n-1})}. \tag{35}$$

Since $\tilde{r}$ involves the ratio of energy spacings, the advantage of evaluating $\tilde{r}$ is that it is independent of the local density of states. The definition in Eq. (35) implies that it is restricted to lie in the range 0 to 1.The average value of $\tilde{r}$ turns out to be 0.34 for integrable models but close to 0.53 for nonintegrable models governed by the Wigner-Dyson Gaussian orthogonal ensemble (GOE). For our model, we evaluate $\tilde{r}$ in a particular sector $(D_1, D_2, D_3) = (1, -1, -1)$ and with open boundary conditions to eliminate degeneracies due to any residual global symmetries. For $L = 18$, we obtain the value of the average of $\tilde{r}$ to be 0.533. We further see that the numerical data fits very well to the Wigner-Dyson distribution of $P(\tilde{r})$ given by [62]

$$P(\tilde{r}) = \frac{27}{4}\frac{r + r^2}{(1 + r + r^2)^{5/2}}\Theta(1 - r), \tag{36}$$

where $r_n = s_n/s_{n-1}$ and $\Theta(x)$ is the usual theta function. In Fig. 7, we see that the distribution given in Eq. (36) matches very well with the numerical data. This establishes that the three-spin model is nonintegrable. Given that it is nonintegrable, we find some of the energy eigenstates with zero energy have an interesting feature as will be discussed in the section below.

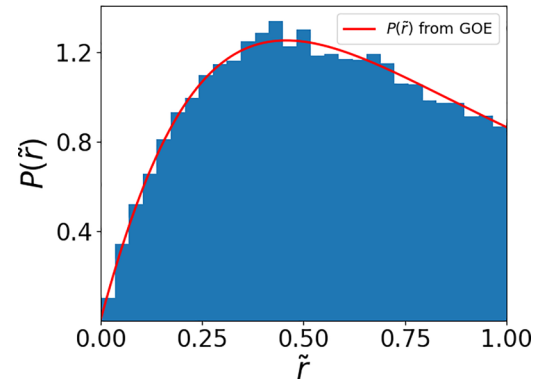

FIG. 7. The distribution of $\tilde{r}$ defined in Eq. (35) is plotted for system size $L = 18$ with open boundary conditions in the sector $(D_1, D_2, D_3) = (1, -1, -1)$ that contains 65 536 eigenstates. Further the expected distribution derived for a GOE $P(\tilde{r})$ is shown in red. We see that they agree quite well. The average of $\tilde{r}$ also turns out to be close to 0.53 as expected for GOE.

B. Zero-energy states

An the interesting property of the three-spin model is that for even system sizes with PBC, we find a large number of states with $E = 0$. These are mid-spectrum states since we have a $E \to -E$ symmetry of the energy levels. We find that the number of zero-energy increases with system size at least as fast as $2^{L/2}$. We can prove this using an index theorem [15]. Writing the Hamiltonian H_3 in the σ^y basis we find that it can be made to have only off-diagonal blocks when the states are divided into two sectors as follows. The spin states for a system size of L is divided into sectors of (i) states with the number of spin states with $\sigma^y = +1$ being even, labeled as $N_{\uparrow,\text{even}}$ (ii) states with the number of spin states with $\sigma^y = +1$ being odd labeled as $N_{\uparrow,\text{odd}}$. This is because for states in $N_{\uparrow,\text{even}}$, the first term in H_3 will flip spins on three sites in the state and the second term will flip one spin, both giving a state with an odd number of up spins, thus connecting to the sector of $N_{\uparrow,\text{odd}}$. The index theorem states that the number of zero-energy states in the system is equal to or greater than the absolute value of the difference in the number of states in each sector, thus giving a lower bound on the number of zero-energy states. In this case, however, we find that $|N_{\uparrow,\text{even}} - N_{\uparrow,\text{odd}}| = 0$. However we see that the parity operator can be used to further divide these two sectors into states with $P = \pm 1$. Since L is even, we define parity as reflection about the middle of the $(\frac{L}{2})$th and $(\frac{L}{2} + 1)$th sites and find the number of states with parity $P = \pm 1$ in the two sectors $N_{\uparrow,\text{even}}$ and $N_{\uparrow,\text{odd}}$. Let n_1 be the number of states with $(P = 1, N_{\uparrow,\text{even}})$, n_2 with $(P = 1, N_{\uparrow,\text{odd}})$, n_3 with $(P = -1, N_{\uparrow,\text{even}})$, and n_4 with $(P = -1, N_{\uparrow,\text{odd}})$. We know the following relations between n_1, n_2, n_3, and n_4.

$$\begin{aligned} n_1 + n_2 + n_3 + n_4 &= 2^L, \\ n_1 + n_3 = n_2 + n_4 &= 2^{L-1}. \end{aligned} \tag{37}$$

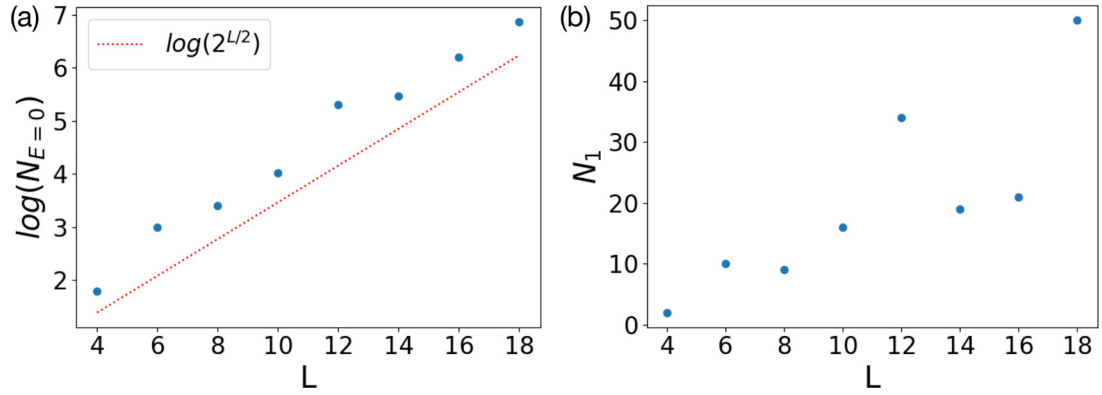

FIG. 8. (a) Plot of logarithm of total number of zero-energy states $N_{E=0}$ versus the system size L. For all L, we see that it is greater than $2^{L/2}$ which is a bound given by an index theorem. (b) Plot of the total number N_1 of type-I states versus L. This number also generally increases with system size although not monotonically.

Next, given the spin configuration in one of the states, we can see that there are two possibilities. For the system size with L sites, we can have the configuration from site numbers 1 to $L/2$ to be either (i) different from or (ii) same as the configuration from sites L to $(L/2)+1$. Examples of this for $L=6$ are as follows. For the first type, an example of such a configuration is a state like $|\psi\rangle = |\uparrow\uparrow\downarrow\uparrow\downarrow\uparrow\rangle$ for which we see that the spins from 1 to 3 are not the same as from 6 to 4. For such states we can take superpositions $|\psi\rangle + P|\psi\rangle$ and $|\psi\rangle - P|\psi\rangle$ which are eigenstates of P with eigenvalues $+1$ and -1, respectively. These two come in equal numbers for all $|\psi\rangle$. An example of the second type of configuration is $|\uparrow\uparrow\downarrow\downarrow\uparrow\uparrow\rangle$ where the reflection about the midpoint has the same configuration on either side. Such states therefore are eigenvectors of the parity operator with eigenvalue $+1$, i.e., $P|\psi\rangle = \psi$. We also note that such states have to belong to the sector $N_{\uparrow,\text{even}}$ since the total number of up- pointing spins is always twice the number of them till half the lattice. From this, we can conclude that the total number of such states of second type are equal to the difference between the number of $N_{\uparrow,\text{even}}$ with $P=1$ and $P=-1$. It is also equal to the number of ways of selecting the configuration from sites 1 to $L/2$, since the other half is then fixed by mirror reflection. This gives $2^{L/2}$, which leads to the relation

$$n_1 - n_3 = 2^{L/2}. \tag{38}$$

Turning to the sector $N_{\uparrow,\text{odd}}$, we see that no state can have $P|\psi\rangle = \pm|\psi\rangle$. The combination $|\psi\rangle + P|\psi\rangle$ and $|\psi\rangle - P|\psi\rangle$ again gives equal number of states with eigenvalues ± 1. This further implies that

$$n_2 = n_4. \tag{39}$$

From Eqs. (37)–(39), we have the following expressions for the numbers of states in the four sectors:

$$\begin{aligned} n_1 &= \tfrac{1}{2}(2^{L-1} + 2^{L/2}), \\ n_2 &= \tfrac{1}{2}2^{L-1}, \\ n_3 &= \tfrac{1}{2}(2^{L-1} - 2^{L/2}), \\ n_4 &= \tfrac{1}{2}2^{L-1}. \end{aligned} \tag{40}$$

Thus considering the parity sector $P=+1$, we see that a lower bound for the number of zero-energy states is given by $|n_1 - n_2| = \frac{1}{2}2^{L/2}$, and similarly for $P=-1$, we have $|n_3 - n_4| = \frac{1}{2}2^{L/2}$. Adding these up we see that the total number of zero-energy states for this system must satisfy $N_{E=0} \geqslant 2^{L/2}$. We plot the total number of zero-energy states as a function of L in Fig. 8(a). We indeed see that the number is greater than the lower bound of $2^{L/2}$ for all values of L.

C. Type-I and type-II zero modes

We now notice something more interesting about the zero-energy states described in Sec. V B. We again consider the Hamiltonian written in the form given in Eq. (8). It then turns out that the zero-energy states come in two types, type-I and type-II. A given zero-energy state $|\psi\rangle$ is said to be type-II if $H_3|\psi\rangle = 0$ but the two terms separately do not give zero, i.e., $Z|\psi\rangle \neq 0$ and $X|\psi\rangle \neq 0$. However for a few of the zero-energy states, it turns out that the terms individually also give zero eigenvalues, that is, $Z|\psi\rangle = 0$ and $X|\psi\rangle = 0$. This means that the wave functions of these states are independent of the transverse field h. These type-I zero modes violate the ETH since they remain unchanged as the coupling h is varied in spite of the energy level spacing in their neighborhood being exponentially small in L [18] and can, therefore, be classified as quantum many-body scars [23]. The number of these type-I zero-energy states N_1 also increases with system size as shown in Fig. 8(b). We do not know precisely how fast N_1 grows with the system size L, but we will show below that the growth is at least linear. The speciality of the type-I states becomes more clear when we look at a plot of the half-chain entanglement entropy versus the energy spectrum of this model. We find that most of the states lie close to the thermal entropy of the system except for some states which stand out at $E=0$. These are the type-I zero-energy states which turn out to typically have very low entanglement entropy compared to a generic state close to $E=0$ showing a violation of the ETH [64,65]. For a given system size, we can further perform a minimization of the entanglement entropy within the subspace of these scar states [20] using the algorithm outlined in Ref. [66]. We show these plots with the full spectrum

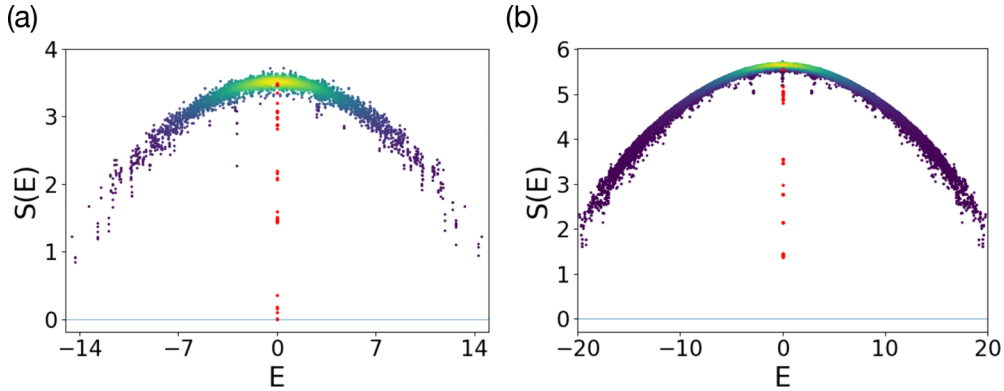

FIG. 9. Plots of the half-chain entanglement entropy spectrum for all the energy levels of the system for $L = 12$ and 18 are shown in (a) and (b), respectively. The plot in red correspond to the type-I scar states which have entanglement entropy much lower than the neighboring states, clearly violating the ETH.

along with the entanglement-entropy minimized scar states in Figs. 9(a) and 9(b), for system sizes $L = 12$ and $L = 18$. We see that there is a dramatic drop in the entropy for most of these scar states confirming that they indeed violate the ETH.

The total number of zero-energy states and the number of type-I zero-energy states for various system sizes L are shown in Table II. We see that the total number of zero-energy states increases rapidly with L while the number of type-I states changes nonmonotonically but on the average increases with L.

We can further appreciate the difference between type-II and type-I states by studying their distribution over the Fock space. A state can be written as a superposition of the basis states of the entire Fock space. A particular scar state, after it has been minimized for entanglement entropy, can be written as $|\psi_S\rangle = \sum_n^{2^L} c_n |\psi_n\rangle$, where $|\psi_n\rangle$ are the basis states in the Fock space and c_n is the corresponding amplitude for the scar state $|\psi_S\rangle$. In Fig. 10, we plot the probability $|c_n|^2$ for a generic zero-energy state and for the scar states. We see that a type-II state [Fig. 10(a)] has nonzero coefficients over a large number of basis states, and the distribution looks random. However, type-I states as shown in Figs. 10(b) and 10(c) can be easily distinguished as they have a large weight over only a few basis states with equal probabilities.

An interesting feature of the type-I states is that since they are annihilated simultaneously by the operators X and Z and are therefore zero energy eigenstates of the Hamiltonian H_3 for any value of h, they will not evolve with time even if h varies with time in an arbitrary way. In particular, if h is taken to vary periodically with a time period T, the type-I states will be eigenstates of the Floquet operator U_T which evolves the system over one time period, and the eigenvalue will be exactly equal to 1. While examples of quantum many-body scars has been found in driven systems for specific driving protocols [67–72], these type-I states provide examples of scars for any driving protocol $h(t)$. Similarly, if the value of h is suddenly changed from one value to another (called a quench), these states will not change. Finally, if h is held fixed and we initialize the system in one of these states (or in an arbitrary linear combination of them), the system will stay in that state for all times, namely, the system will not thermalize.

TABLE II. Total number of zero-energy states and number of type-I zero-energy states for various system sizes.

System size L	Total number of zero-energy states	Number of type-I states
4	6	2
6	20	10
8	30	9
10	56	16
12	202	34
14	236	19
16	492	21
18	970	50

D. Some exact type-I states

We will now present some type-I states (scars) which we have found analytically [73]. To this end, let us define two states involving sites j and k given by

$$S_{j,k} = \frac{1}{\sqrt{2}}(|\uparrow_j\downarrow_k\rangle - |\downarrow_j\uparrow_k\rangle),$$
$$T_{j,k} = \frac{1}{\sqrt{2}}(|\uparrow_j\downarrow_k\rangle + |\downarrow_j\uparrow_k\rangle), \tag{41}$$

where $\uparrow$ and $\downarrow$ denote spin-up and spin-down in the σ^x basis. These are, respectively, spin-singlet and spin-triplet states with total $S^x = (\sigma_j^x + \sigma_k^x)/2 = 0$. Note that these states are antisymmetric and symmetric respectively under the exchange of sites j and k. We find that they satisfy the identities

$$\sigma_j^z S_{j,k} = -\sigma_k^z S_{j,k}, \quad \sigma_j^z\sigma_k^z S_{j,k} = -S_{j,k},$$
$$\sigma_j^z T_{j,k} = \sigma_k^z T_{j,k}, \quad \sigma_j^z\sigma_k^z T_{j,k} = T_{j,k}. \tag{42}$$

We now consider a system with L sites with PBC and a state which is a product of singlets with the form

$$|\psi_1\rangle = S_{L,1}S_{L-1,2}S_{L-2,3}\cdots S_{(L/2)+1,L/2}. \tag{43}$$

Clearly $X|\psi\rangle = 0$ where the operator X is given in Eq. (8). [A picture of $|\psi_1\rangle$ for $L = 8$ is shown in Fig. 11(a)]. Each line connecting a pair of sites denotes a spin-singlet state).

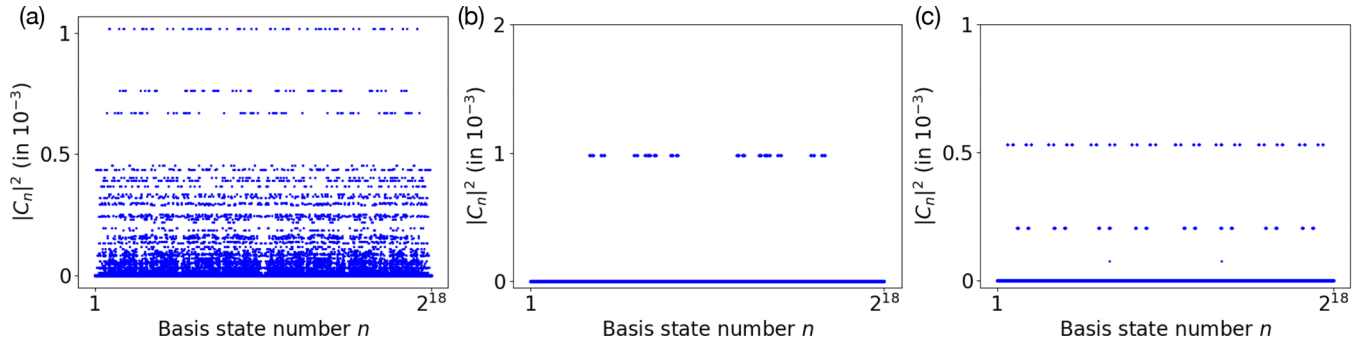

FIG. 10. (a) Probabilities $|c_n|^2$ of a generic type-II $E = 0$ state in the entire Fock space for all the basis states are plotted for $L = 18$. We see that the distribution is random. (b) and (c) show the same plot for different type-I scar states. The distribution is more sparse and also has equal probabilities for many basis states.

Equations (42) then imply that

$$\begin{aligned}
\left(\sigma^z_{L-1}\sigma^z_L\sigma^z_1 + \sigma^z_L\sigma^z_1\sigma^z_2\right)|\psi_1\rangle &= 0,\\
\left(\sigma^z_{L-2}\sigma^z_{L-1}\sigma^z_L + \sigma^z_1\sigma^z_2\sigma^z_3\right)|\psi_1\rangle &= 0,\\
\left(\sigma^z_{L-3}\sigma^z_{L-2}\sigma^z_{L-1} + \sigma^z_2\sigma^z_3\sigma^z_4\right)|\psi_1\rangle &= 0,\\
&\cdots\\
\left(\sigma^z_{L/2+1}\sigma^z_{L/2+2}\sigma^z_{L/2+3} + \sigma^z_{L/2-2}\sigma^z_{L/2-1}\sigma^z_{L/2}\right)|\psi_1\rangle &= 0,\\
\left(\sigma^z_{L/2}\sigma^z_{L/2+1}\sigma^z_{L/2+2} + \sigma^z_{L/2-1}\sigma^z_{L/2}\sigma^x_{L/2+1}\right)|\psi_1\rangle &= 0. \qquad (44)
\end{aligned}$$

Hence the state $|\psi\rangle$ satisfies $Z|\psi\rangle = 0$ where the operator Z is given in Eq. (8). Since both X and Z annihilate $|\psi\rangle$, we conclude that this is a type-I state.

Next, we can take the state $|\psi_1\rangle$ and rotate all the sites clockwise by 1 site on the circle. This gives the state

$$|\psi_2\rangle = S_{1,2}S_{L,3}S_{L-1,4}\cdots S_{(L/2)+2,(L/2)+1}, \qquad (45)$$

and following similar arguments we can show that $|\psi_2\rangle$ is also a type-I state. Continuing in this way, we find $L/2$ distinct states, denoted $|\psi_n\rangle$, $n = 1, 2, \cdots, L/2$, which are all type-I states.

Now we observe that if the system is cut into two equal parts by a line, and we consider the state $|\psi_1\rangle$, the line may cut no singlets, one singlet, two singlets, and so on all the way up to $L/2$ singlets, depending on the orientation of the line [see the two dashed lines in Fig. 11(a)]. As a result, the half-chain entanglement entropy can take all possible values from zero up to $(L/2)\ln 2$. Even the largest of these values is only half of the thermal entropy given by $L\ln 2$. This again confirms that these are all scar states. We note that the state shown in Fig. 11(a) resembles the rainbow scars discussed in Ref. [74].

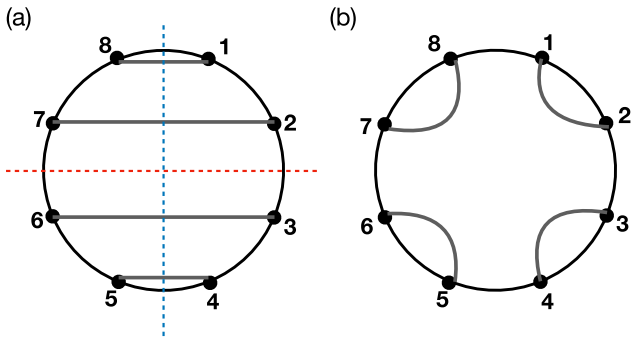

FIG. 11. (a) Picture of the state $|\psi_1\rangle$ given in Eq. (43) for $L = 8$. The lines joining pairs of sites denote spin singlets. Two straight lines dividing the system into two equal parts are shown by dashed lines. The vertical dashed line cuts $L/2$ singlets, while the horizontal dashed line does not cut any singlet; thereby producing half-chain entanglement entropies equal to $(L/2)\ln 2$ and zero respectively. (b) Picture of the state $|\phi_1\rangle$ given in Eq. (46).

It turns out that there are two other singlet states, denoted $|\phi_1\rangle$ and $|\phi_2\rangle$, which are also type-I states. These have the form

$$\begin{aligned}
|\phi_1\rangle &= S_{1,2}S_{3,4}S_{5,6}\cdots S_{L-1,L},\\
|\phi_2\rangle &= S_{2,3}S_{4,5}S_{6,7}\cdots S_{L,1}. \qquad (46)
\end{aligned}$$

[A picture of $|\phi_1\rangle$ is shown in Fig. 11(b)]. Using Eqs. (42), we can show that these states are also annihilated by the operator Z. (As before, we can find pairs of three-spin terms $\sigma^z_i\sigma^z_j\sigma^z_k$ and $\sigma^z_l\sigma^z_m\sigma^z_n$ such that the sum of the two terms annihilates the states $|\phi_n\rangle$). Further, the half-chain entanglement entropy for these two states range from zero to $2\ln 2$ depending on the orientation of the line which cuts the system into two halves.

For $L = 4$, the states ψ_n and ϕ_n are identical, and we therefore have only two exact type-I states; according to Table II, these form the complete set of type-I states. For $L \geqslant 6$, the states ψ_n and ϕ_n are distinct, and we therefore have $(L/2) + 2$ type-I states.

The states $|\psi_n\rangle$ and $|\phi_n\rangle$ discussed above are examples of resonating valence bond (RVB) states for a L-site system. If the L sites are arranged around a circle, the RVB states correspond to joining pairs of sites by lines in such a way that no two lines cross each other. According to the Rumer-Pauling rules [75], there are $L!/(L/2)!((L/2)+1)!$ such states which are linearly independent, although not orthogonal to each other. We see that $(L/2) + 2$ of the RVB states are type-I states for our model. We conclude that the number of type-I states increases at least linearly with L.

We can construct one more type-I state using singlet states as follows. For a system with L sites and PBC, consider the following state which is a product of singlets connecting diametrically opposite sites,

$$|\psi_d\rangle = S_{1,(L/2)+1}S_{2,(L/2)+2}S_{3,(L/2)+3}\cdots S_{L/2,L}. \qquad (47)$$

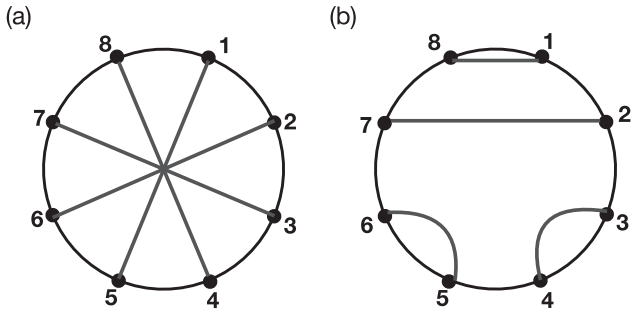

FIG. 12. (a) Picture of the state $|\psi_d\rangle$ given in Eq. (47) for $L = 8$. The lines joining pairs of diametrically opposite sites denote spin singlets. (b) Picture of the state $|\phi_d\rangle$ given in Eq. (49).

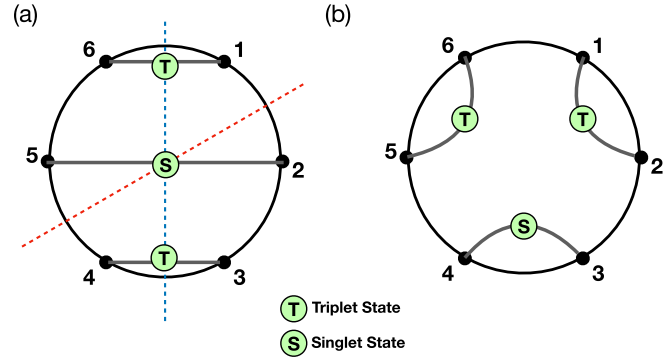

FIG. 13. (a) Picture of the state $|\psi_1'\rangle$ given in Eq. (50) for $L = 6$. The lines joining pairs of sites denote spin singlets or triplets shown as S or T respectively. The dashed lines divide the system into two equal parts and they cut one and three bonds respectively. (b) Picture of the state $|\phi_1'\rangle$ given in Eq. (51).

We find that this state is annihilated by terms of the form $\sigma_n^z\sigma_{n+1}^z\sigma_{n+2}^z + \sigma_{(L/2)+n}^z\sigma_{(L/2)+n+1}^z\sigma_{(L/2)+n+2}^z$, where $n = 1, 2, \ldots, L/2$. Hence $|\psi_d\rangle$ is annihilated by the operator Z given in Eq. (8). A picture of $|\psi_d\rangle$ for $L = 8$ is shown in Fig. 12(a). However, $|\psi_d\rangle$ is not an RVB state since the different singlet lines cross each other; in fact, any two singlet lines cross each other. However, we can write $|\psi_d\rangle$ as a linear combination of RVB states by using the identity

$$S_{i,j}S_{k,l} - S_{i,k}S_{j,l} + S_{i,l}S_{j,k} = 0 \tag{48}$$

several times. Depending on how four sites labeled i, j, k, l are arranged around a circle, one of the terms in Eq. (48) will corresponding to a state with one crossing while the other two terms will correspond to noncrossing states. Hence, by repeatedly using Eq. (48), we can successively decrease the number of crossings to eventually reduce $|\psi_d\rangle$ to a superposition of RVB states. For $L = 8$, we find that the superposition contains all the states shown in Figs. 11(a) and 11(b) as well as a *specific* linear combination of eight other RVB states which are of the form

$$|\phi_d\rangle = S_{1,8}S_{2,7}S_{3,4}S_{5,6}, \tag{49}$$

shown in Fig. 12(b), and seven other states obtained from Eq. (49) by rotating all the sites clockwise by 1, 2, ..., 7 sites.

The different kinds of exact type-I states discussed above do not exhaust all the type-I states. For instance, Table II shows that there are 9 type-I states for $L = 8$, but the arguments above only account for $(L/2) + 2 + 1 = 7$ of them.

Finally, we note that if L is a multiple of 6, we can find exact type-I states involving both singlets and triplets. Two such states are shown in Fig. 13 for a system with six sites. The state in Fig. 13(a) has the form

$$|\psi_1'\rangle = T_{6,1}S_{5,2}T_{4,3}, \tag{50}$$

while the state in Fig. 13(b) has the form

$$|\phi_1'\rangle = T_{1,2}S_{3,4}T_{5,6}. \tag{51}$$

These can be shown to be type-I states by similar arguments as above and using the identities in Eqs. (42). Then one can repeatedly rotate all the sites by 1 site from $|\psi_1'\rangle$ and $|\phi_1'\rangle$ obtain states of the form $|\psi_n'\rangle$, $n = 1, 2, 3$, and $|\phi_n'\rangle$, $n = 1, 2, \ldots, 6$, respectively. We thus obtain nine states each of which involves one singlet and two triplets. However, one can show that only five of these states are linearly independent; one can choose these to be of the form $|\phi_n'\rangle$, where $n = 1, 2, \ldots, 5$. For $L = 6$, therefore, we get $(L/2) + 2 = 5$ states involving only singlet states and five state involving both singlets and triplets. This gives a total of 10 type-I states for $L = 6$ which is in agreement with Table II.

A similar construction of type-I states involving singlets and triplets exists whenever L is a multiple of 6. There are two kinds of such states. The first kind of states resembles the one shown in Fig. 13(a) and is given by

$$|\psi_1'\rangle = T_{L,1}S_{L-1,2}T_{L-2,3}T_{L-3,4}\cdots S_{L-4,5} \cdots T_{L/2+3,L/2-2}S_{L/2+2,L/2-1}T_{L/2+1,L/2}, \tag{52}$$

and similar states obtained by rotating all the sites by 1 site. The pattern of bonds from the top to the bottom follows the pattern $TSTTSTT\cdots STTST$. There are $L/2$ states of this kind. The second kind of states resembles the one shown in Fig. 13(b) and is given by

$$|\phi_1'\rangle = T_{1,2}S_{3,4}T_{5,6}T_{7,8}S_{9,10}T_{11,12} \cdots T_{L-5,L-4}S_{L-3,L-2}T_{L-1,L}, \tag{53}$$

and similar states obtained by rotating all the sites by 1 site. The bonds follow the pattern $TSTTSTT\cdots STTST$ around the circle. There are six states of this kind. We therefore have a total of $(L/2) + 6$ type-I states, each of which is a product of $L/6$ singlets and $L/3$ singlets. However, unlike the type-I states which involve only singlets where we found that there are $(L/2) + 2$ linearly independent states, we do not know how many of the $(L/2) + 6$ type-I states involving singlets and triplets are linearly independent for a general value of L. For $L = 6$, we saw above that the number of independent states is 5, but a formula for $L = 12, 18, 24, \ldots$ is not known.

Once again, we note that when the system is cut into two equal parts by a line, the number of bonds (singlets or triplets) cut by the line can vary from zero to $L/2$ depending on its orientation [see Fig. 13(a)]. The half-chain entanglement entropy can therefore vary from zero up to $(L/2)\ln 2$ which is much smaller than the thermal entropy equal to $L\ln 2$.

The fact that there are several exact type-I states involving singlets and triplets which appear only when L is a multiple

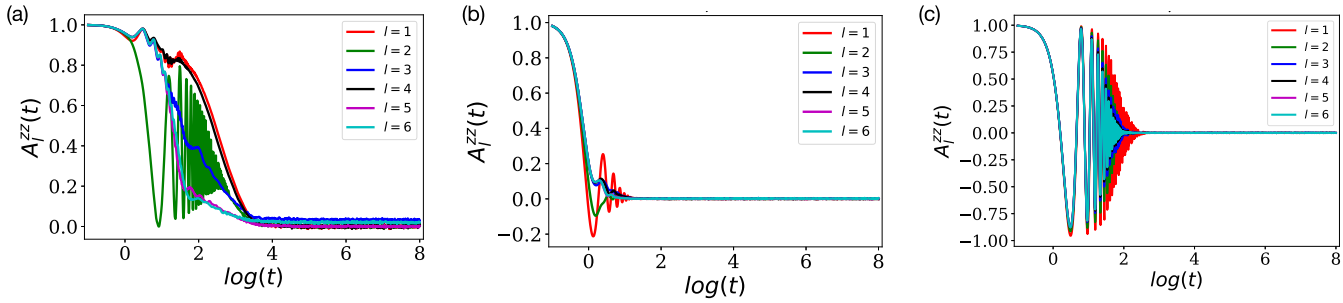

FIG. 14. Autocorrelation function $A_l^{zz}(t)$ for $L = 14$ plotted versus time on a log scale for different values of the transverse field. Deep inside the ordered phase, (a) $h = 0.2$, or the disordered phase, (c) $h = 5$, the autocorrelators at several sites near the boundary show oscillations for a long time before decaying to zero. (b) At the critical point, $h = 1$, the autocorrelators decay quickly to zero at all sites except at the boundary site.

of 6 may help to explain why there is a jump in the number of type-I states whenever L hits those particular values, as we can see in Table II.

It would be interesting to find all possible type-I states exactly but this seems to be a difficult problem. We note that all the exact type-I states discussed in this section have been found by demanding that they be annihilated by the sum of two three-spin terms of the form $\sigma_i^z\sigma_j^z\sigma_k^z + \sigma_l^z\sigma_m^z\sigma_n^z$, and these sums combine to give the total operator Z in Eq. (8). However, there may be more complicated type-I states which are only annihilated by the sum of three or more three-spin terms.

It is intriguing that singlets and triplets (with zero magnetization) play such an important role in the construction of type-I states even though the Hamiltonian H_3 is not invariant under $SU(2)$ or any other continuous symmetry.

VI. ANOMALOUS RELAXATION OF AUTOCORRELATORS AT DIFFERENT SITES

The ordered phase of the TFIM on a semi-infinite system is characterized by a doubly degenerate spectrum and the presence of a strong edge mode operator that connects pairs of degenerate states with opposite parity [29,30]. Numerically, this can be observed by studying the infinite-temperature autocorrelator of the σ^z operator at different sites near the edge of the system [31–33].

$$A_l^{zz}(t) = \frac{1}{2^L}\mathrm{Tr}\left[\sigma_l^z(t)\sigma_l^z\right]. \tag{54}$$

Since the strong mode operator has a large overlap with the operator σ_1^z operator at the boundary site, the autocorrelator shows a long plateau near the value of unity with a time scale that increases exponentially with the system size before relaxing to zero. However the autocorrelator of σ^z at any other site falls off to zero very quickly in a time scale $t \lesssim 10$.

This motivates us to ask a similar question for the nonintegrable model H_3 with open boundary conditions. As discussed earlier, this model has an exact degeneracy in three-fourths of its eigenstates due to the presence of the D_1, D_2, D_3 operators for PBC, and also a twofold degeneracy in half of its eigenstates due to parity symmetry for open boundary conditions. These degeneracies are present for any value of the transverse field h. We will study how the spin autocorrelators relax in time at sites near the boundary for various values of h and see if the degeneracies play any role in the relaxation. The infinite-temperature autocorrelators can be calculated as traces over all the energy eigenstates of the Hamiltonian. We will be interested in the zz and xx autocorrelators given by

$$A_l^{zz}(t) = \frac{1}{2^L}\sum_{n,m} e^{i(E_n-E_m)t}\left|\langle n|\sigma_l^z|m\rangle\right|^2 \tag{55}$$

and

$$A_l^{xx}(t) = \frac{1}{2^L}\sum_{n,m} e^{i(E_n-E_m)t}\left|\langle n|\sigma_l^x|m\rangle\right|^2, \tag{56}$$

respectively. The autocorrelators defined in this way are expected to reveal the nature of the phase transition and the energy spectra on the two sides of the transition.

We present the results for $A_l^{zz}(t)$ versus t on a logarithmic scale for different lattice sites $l = 1, 2, \ldots 6$ (with $l = 1$ being the boundary site) and three values of the transverse field, $h = 0.2,\ 1,$ and 5.0, in Figs. 14(a), 14(b) and 14(c), respectively. The relaxation of the autocorrelators shows very interesting behaviors depending on whether $h \ll 1$, $h \gg 1$ or $h = 1$. For $h = 0.2$ [see Fig. 14(a)], we observe qualitatively that A_1^{zz} and A_4^{zz} have a similar structure, with a small plateau for a time interval of $t \lesssim 10^4$, where the autocorrelator remains near 1 before falling off to zero at large times. We believe that this is due to the presence of an operator, which has an appreciable overlap with σ^z at sites 1 and 4 and also has a small commutator with the Hamiltonian itself. The autocorrelator at site $l = 2$ has the most striking behavior, showing oscillations with an approximate period of 15.5. We also plot the same autocorrelator in real time instead of the logarithmic scale in Fig. 15(a), where the oscillations can be seen clearly.

The small frequency oscillations at the site $l = 2$ can be explained by considering the Hamiltonian in the small h limit and doing a perturbative calculation. First, by putting $h = 0$, we have the Hamiltonian given by $H_3|_{h=0} = Z = -\sum_{j=1}^{L-2}\sigma_j^z\sigma_{j+1}^z\sigma_{j+2}^z$. The eigenstates of this are given by product states where each site j has a definite value of $\sigma_j^z = \pm 1$. Therefore, all the eigenvalues of Z are integer valued and so are the energy differences. Now, an introduction of a small value of transverse field h gives eigenstates with energy differences of order h. To see this, we look at the couplings in the Z term and the effects of σ_l^z in the autocorrelator more carefully. The couplings in Z containing a

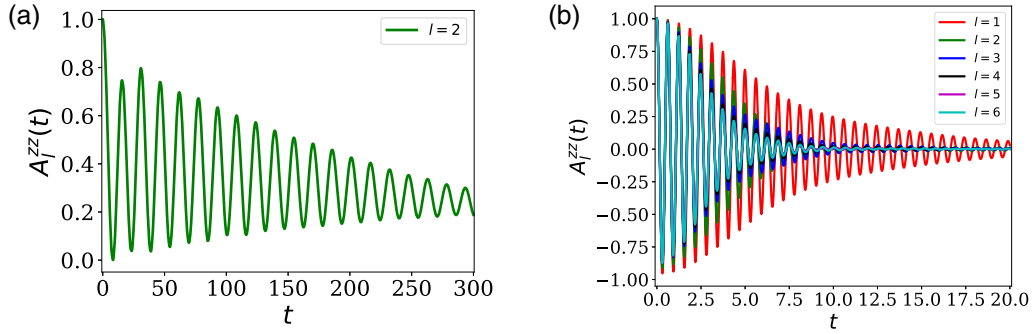

FIG. 15. (a) $A_l^{zz}(t)$ at site $l = 2$ for $h = 0.2$, showing long-time oscillations. This can be understood using first-order degenerate perturbation theory. (b) $A_l^{zz}(t)$ showing oscillations at different sites for $h = 5$. This can be understood using effective two-level systems. Both the figures are for system size $L = 14$.

particular σ_l^z can be considered for three separate cases, (a) $\sigma_l^z(\sigma_2^z\sigma_3^z)$, for $l = 1$, (b) $\sigma_l^z(\sigma_1^z\sigma_3^z + \sigma_3^z\sigma_4^z)$, for $l = 2$, and (c) $\sigma_l^z(\sigma_{l-2}^z\sigma_{l-1}^z + \sigma_{l-1}^z\sigma_{l+1}^z + \sigma_{l+1}^z\sigma_{l+2}^z)$, for $l \geqslant 3$. Since each σ_j^z can take values ± 1, the products of two spin operators also will take values ± 1. Therefore, in cases (a) and (c), we have a sum of an odd number of such products which necessarily has a nonzero value. However, in case (b), we have an even number of such terms and hence, for $l = 2$, we can have a case where σ_2^z is multiplied by zero. More precisely, this happens if $\sigma_3^z(\sigma_1^z + \sigma_4^z) = 0$, i.e., if $(\sigma_1^z + \sigma_4^z) = 0$. Thus the two sets of eigenstates of Z corresponding to the value of $\sigma_2^z = \pm 1$ (we label them as $|I\rangle$ and $|II\rangle$ respectively) will be degenerate for any values of $\sigma_1^z, \sigma_3^z, \sigma_4^z, \sigma_5^z, \sigma_6^z, \ldots$, with the condition that $(\sigma_1^z + \sigma_4^z) = 0$. This condition is satisfied for half of the states when σ_1^z and σ_4^z are opposite to each other, and then we have a pairwise degeneracy between the states of types $|I\rangle$ and $|II\rangle$. With a small h present, the term $-h\sigma_2^x$ will break the degeneracy, since $\sigma_2^x\,|I\rangle = |II\rangle$ and vice versa. Therefore we end up having a new set of eigenstates $|\pm\rangle = 1/\sqrt{2}(|I\rangle \pm |II\rangle)$ with an energy splitting of $2h$. Now, since $\langle -|\,\sigma_2^z\,|+\rangle = 1$, we see from Eq. (55) that for $l = 2$, half the states of the spectrum in the autocorrelator will contribute to a oscillatory term $e^{\pm i2ht}$. This exactly explains the oscillations seen in Fig. 15(a). Eventually, for later times the oscillations decay as terms of order h^2 and higher in the energy differences become important.

We also note that since $|\pm\rangle$ are eigenstates of σ_2^x, with eigenvalues ± 1, these states will contribute to the diagonal terms (i.e., terms with $m = n$ and therefore $E_m = E_n$) in the xx autocorrelator at $l = 2$ in Eq. (56). Since the diagonal terms are time-independent (as $E_m = E_n$), we expect that the xx autocorrelator at $l = 2$ will have a nonzero constant term. This agrees with what we see in Fig. 16(a) for $h = 0.2$.

For large values of h, we see in Fig. 15(b) that at several sites near one end of the system, the zz autocorrelators show pronounced oscillations before eventually decaying to zero. All the oscillations have the same frequency which is found to be close to $2h$. We can understand this as follows. For $h \gg 1$, we see from Eq. (2) that the eigenstates of H are given, to lowest order, by products of eigenstates of σ_j^x for all j. An operator σ_j^z connects two states which have $\sigma_j^x = \pm 1$ and therefore unperturbed energies equal to $\mp h$. The energy difference of these two states is $2h$, hence Eq. (55) implies that the contribution of these two states to the zz autocorrelator at site j will oscillate as $e^{\pm i2ht}$; this explains Fig. 15(b). Next, we can extend this argument to first order in perturbation theory. Consider the zz autocorrelator at the first site given by $j = 1$ where the oscillations are most pronounced. To first order in the perturbation $V = -\sigma_1^z\sigma_2^z\sigma_2^z$, the two states given by $|I\rangle = |\sigma_1^x = +1, \sigma_2^x = a, \sigma_3^x = b\rangle$ and $|II\rangle = |\sigma_1^x = -1, \sigma_2^x = -a, \sigma_3^x = -b\rangle$ will mix (here a, b can take values ± 1). The unperturbed energies of these states are $E_I = -h(1 + a + b)$ and $E_{II} = h(1 + a + b)$, respectively. Hence, to first order in perturbation theory, the energy of the state lying close to $|I\rangle$ will shift from $E_I = -h(1 + a + b)$ to $E_I' = -h(1 + a + b) + 1/(E_I - E_{II}) = -h(1 + a + b) - 1/(2h(1 + a + b))$. Similarly, the perturbation V mixes the two states $|III\rangle = |\sigma_1^x = -1, \sigma_2^x = a, \sigma_3^x = b\rangle$ and $|IV\rangle = |\sigma_1^x = 1, \sigma_2^x = -a, \sigma_3^x = -b\rangle$, and shifts the energy of the state lying close to $|III\rangle$ from $E_{III} = h(1 - a - b)$ to $E_{III}' = h(1 - a - b) + 1/(2h(1 - a - b))$. The operator σ_1^z connects the states lying close to $|I\rangle$ and $|III\rangle$, and we see from the expressions above that the energy difference between these two states is

$$|E_I' - E_{III}'| = 2h + \frac{1}{2h}\left(\frac{1}{1 + a + b} + \frac{1}{1 - a - b}\right) = 2h + \frac{1}{h}\left(\frac{1}{1 - (a + b)^2}\right). \tag{57}$$

According to Eq. (55), therefore, the oscillations will have the frequency given in Eq. (57). Now, since a, b can independently take the values ± 1, giving rise to four possibilities, the expression in Eq. (57) can take two possible values given by $2h + (1/h)$ (when $a = -b$) and $2h - (1/3h)$ (when $a = b$). Hence we expect the oscillations to have a frequency ω, where $\omega/(2h) = 1 + 1/(2h^2)$ and $1 - 1/(6h^2)$. Since these two cases appear and equal number of times, the average value is given by $\omega/(2h) = 1 + (1/6h^2)$. This is in reasonable agreement with the numerical result shown in Fig. 17 for large values of h. We note that since the frequency ω used in that figure is obtained by calculating the position of the peak of the Fourier transform of the oscillations in Fig. 15(b), the decay of the oscillations leads to a small width around the peak. This width also turns out to be of the order of $1/h$, and we therefore do not see two separate peaks at $\omega = 2h + (1/h)$ and

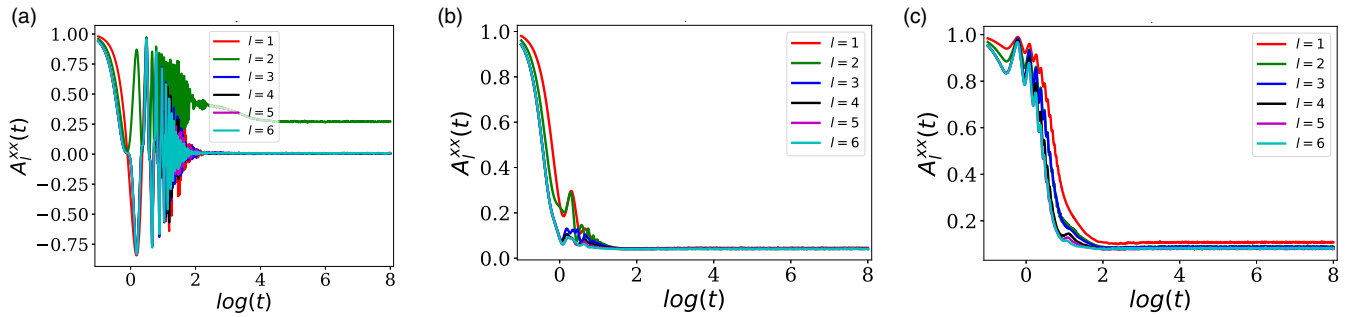

FIG. 16. Autocorrelation function $A_l^{xx}(t)$ for $L = 14$ plotted versus time on a log scale for different values of the transverse field, (a) $h = 0.2$, (b) $h = 1$, and (c) $h = 5$.

$2h - (1/3h)$. Remarkably, these early and intermediate time oscillations in $A_l^{zz}(t)$ persist all the way to $h = 1$ (Fig. 17) for the boundary site when the critical point is approached from $h > 1$, while the other autocorrelators show a reasonably rapid decay in the neighborhood of the critical point (see Appendix C for the extraction of the oscillation frequency ω in Fig. 17).

VII. DISCUSSION

A summary of our main results is as follows. Motivated by the one-dimensional TFIM which is one of the best studied integrable models with duality and a quantum critical point, we have made a detailed study of a generalization in which there are Ising interactions between three successive spins (instead of two successive spins as in the TFIM). We find that the model has a $Z_2 \times Z_2$ symmetry for a system with PBC provided that the system size is a multiple of 3. This symmetry implies that the system consists of four sectors which are decoupled from each other, and this leads to threefold degeneracies in the energy spectrum which involves states from three of the four sectors. Next we have discussed the duality of the model between h and $1/h$. While the duality is straightforward to show for an infinite-sized system, the existence of a duality turns out to be a subtle issue for finite-sized systems with PBC. We find that exact duality holds only if the system size is *not* a multiple of 3. Next, we make a detailed study

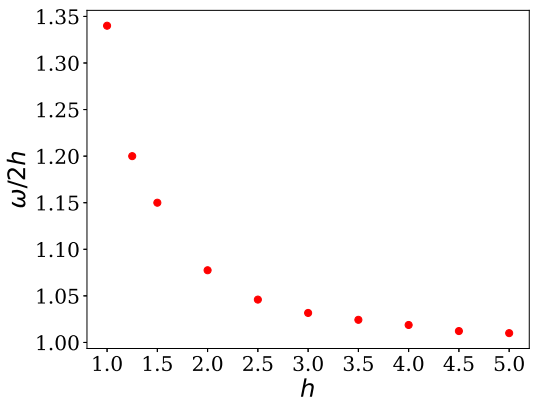

FIG. 17. Variation of the frequency of oscillations of $A_{l=1}^{zz}(t)$ at the end site with the transverse field h for $L = 14$. For large h the dependence is consistent with the perturbative result $\omega/(2h) = 1 + 1/(6h^2)$.

of the criticality properties of the model at the self-dual point given by $h = 1$. Using ED and system sizes up to $L = 27$, we use finite-size scaling to first confirm that there is indeed a critical point at $h = 1$, and then to compute the dynamical critical exponent z, the order parameter exponent β, the magnetic susceptibility exponent γ, and the correlation length exponent ν. We find that $z = 1$ suggesting that the low-energy sector of the model at $h = 1$ has conformal invariance. We then determine the central charge c in two different ways (from the length-dependences of the entanglement entropy between two parts of the system and of the ground state energy). We find that c is close to 1. We then observe that although the values of β, γ and ν for the two-spin and three-spin models are different from each other, the ratios β/ν and γ/ν are the same in the two models. This suggests that there is a weak universality and the three-spin model lies on the AT line, just like two copies of the TFIM and the four-state Potts model. All models on this line are known to have $z = 1$, $c = 1$, and the same values of $\beta/\nu = 1/8$ and $\gamma/\nu = 7/4$. There is a quantum AT model which has a parameter λ such that two copies of the TFIM and the four-state Potts model correspond to $\lambda = 0$ and 1 respectively. Given our numerically obtained value of $\nu \approx 0.75$ for the three-spin model from ED, we estimate this model corresponds approximately to $\lambda \approx 0.7$.

To better understand the nature of the criticality at the self-dual point of the three-spin model, we have used the DMRG method for much longer chains, but with open boundaries. The DMRG method using longer chains indeed confirms that $c = 1$ at the critical point. However, the analysis of the behavior of the smallest excitation gap at $h_c = 1$ and its neighborhood reveals important additive and multiplicative logarithmic corrections. Incorporating these and also comparing to the Ashkin-Teller model at $\lambda = 1$, in fact, shows that the critical point in the three-spin model is likely to lie in the four-state Potts universality class. This claim is further supported by an analysis of the Binder cumulants of the two models. Thus the three-spin model seems to provide a lattice realization of four-state Potts criticality with a smaller Hilbert space dimensionality of 2^L with L sites compared to 4^L for the Ashkin-Teller model.

If the three-spin model and the four-state Potts model indeed lie in the same universality class at their critical points, they should have the same emergent symmetries at that point. We would like to make some observations in favor of this. First, we have seen that the three-spin model with PBC has an exact threefold degeneracy for three-fourth of its states,

namely, states whose momenta differ by multiples of $2\pi/(3d)$ have the same energies (here d is the lattice spacing which we have set equal to 1 in this paper). At the critical point, the lattice model is gapless around $k = 0, 2\pi/(3d)$ and $4\pi/(3d)$. In the continuum theory which describes modes with low energies and wave lengths much larger than d, all the gapless modes of the lattice model at the critical point will get mapped to momenta lying around $k = 0$. We would therefore expect the conformal field theory to have a threefold degeneracy of the low-lying excitations. We now note that this is also the case for the four-state Potts model at criticality since that model has several relevant operators, namely, three with conformal dimensions (1/16, 1/16), one with (1/4, 1/4), and three with (9/16, 9/16), and three marginal operators with conformal dimensions (1,1) [41]. The multiplicities of 3 are expected to lead to threefold degeneracies in the low-lying spectrum [76,77]. Second, we have seen that the three-spin model naturally has three order parameters, (m_A, m_B, m_C), and in the ordered phase, there are four possible ground states in which the expectation values of the order parameters are proportional to (1,1,1), (1, −1, −1), (−1, 1, −1) and (−1, −1, 1); this can be seen most clearly if we consider the limit $h \to 0$ in Eq. (2). These four patterns of the order parameters form a tetrahedron, and the symmetry group of a tetrahedron is the permutation group S_4 of four objects. Next, we note that the four-state Potts model also has a S_4 symmetry [41]. To conclude, the three-spin model at its critical point has the same low-energy degeneracies and the same emergent symmetry as the four-state Potts model.

We then studied the energy level spacing statistics in a particular symmetry sector of a system with open boundary conditions to determine if the three-spin model is integrable. We find that the level spacing statistics has the form of the Gaussian orthogonal ensemble, and hence the model is nonintegrable. Next, we find that the model has an exponentially large number of mid-spectrum zero-energy states which is consistent with an index theorem; the number of states grows at least as fast as $2^{L/2}$. Further, we find that the zero-energy states are of two types which we call type-I and type-II. The type-I states are special because they are simultaneous zero-energy eigenstates of the two parts of the Hamiltonian (the three-spin interaction and the transverse field); hence their wave functions do not change with h in spite of the energy level spacing in their neighborhood being exponentially small in system size. These states thus violate the ETH and qualify as quantum many-body scars. We have presented the analytical forms of some of the type-I states which show that their number grows at least linearly with the system size. However we do not know the form of the growth more precisely (linear, exponential, or some other dependence). Finally, we have studied the infinite-temperature autocorrelation functions for both σ^x and σ^z at sites close to one end of a large system with open boundary conditions. We find that far from the critical point, at either $h \ll 1$ or $h \gg 1$, some of the autocorrelators show an anomalous behavior in that they show pronounced oscillations and decay very slowly with time. The time scale of decay is much larger than the inverse of the energy scales in the Hamiltonian; this is unexpected since the model is nonintegrable. We provide a qualitative understanding of the oscillations using perturbation theory. However, the reason for a large decay time is not yet understood analytically. Furthermore, the autocorrelator for σ^z at the end site shows persistent oscillations at short and intermediate time scales even when h is close to the critical point while the other autocorrelators decay quickly to zero. An analytic understanding of this feature is lacking as of now.

So far as experimental realizations of our three-spin model are concerned, it is known that optical lattices of two atomic species can be a suitable platform to generate a variety of spin-1/2 Hamiltonians. In particular, it has been shown that in a one-dimensional system of triangles formed by an optical lattice, the two-spin interactions can be made to vanish by varying the tunneling and collisional couplings [13]. This gives rise to an effective Hamiltonian with three-spin interactions of the form $\sigma^z_j \sigma^z_{j+1} \sigma^z_{j+2}$. Furthermore, a local field magnetic field $\vec{B}$ can be applied which can be tuned by applying appropriately detuned laser fields which generate a term of the form $B\sigma^x_j$ in the Hamiltonian. It may also be feasible to realize effective Hamiltonians with two- and three-spin terms which are generated by ion-laser interactions in trapped-ion systems [78]. A three-spin NMR quantum simulator based on a diethylfluoromalonate molecule has been used to experimentally realize a system with two- and three-spin Ising interactions [79]. Turning to studies of the scar states, it may be possible to initialize a system in a state which is close to the simplest scar states of the form shown in Figs. 11(b) and 13(b) since these involve preparing only neighboring sites to be in spin-singlet or spin-triplet states, and to then study the time-evolution of such a state.

ACKNOWLEDGMENTS

A.S. thanks H. Katsura for illuminating discussions. D.S. thanks C. Krishnan for stimulating discussions in the early stages of this work. S.N. thanks L. Pavešić and Z. Lenarčič for very useful discussions. A.S. and D.S. acknowledge useful discussions with the participants in the ICTS program titled "Periodically and quasiperiodically driven complex systems" (code: ICTS/pdcs2023/6). S.S. and S.N. thank ICTP in Trieste, Italy for its hospitality during the program titled "School on Quantum Many-Body Phenomena out of Equilibrium: from Chaos to Criticality (smr 3867)." S.S. thanks MHRD, India for financial support through the PMRF. D.S. acknowledges funding from SERB, India through project JBR/2020/000043. S.N. acknowledges the support by the Projects No. J1-2463, No. N1-0318, and No. P1-0044 program of the Slovenian Research Agency and the QuantERA grant T-NiSQ, by MVZI, QuantERA II JTC 2021. The DMRG calculations were performed at the spinon cluster of Jožef Stefan Institute, Ljubljana.

APPENDIX A: BINDER CUMULANT

Here we present another quantity that shows that the critical behavior of the three-spin model is different to that of the TFIM. The Binder cumulant U_2 is defined as [55–57]

$$U_2 = C + D\frac{\langle m^4 \rangle}{\langle m^2 \rangle^2}, \tag{A1}$$

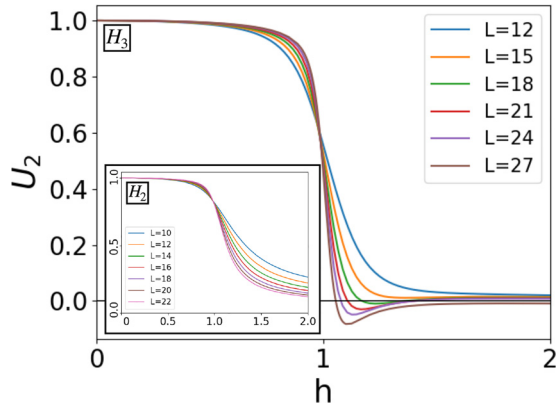

FIG. 18. Plot of Binder cumulant U_2 defined in Eq. (A1) as a function of the field h for the three-spin model. The plots for different system sizes cross each other close to h_c. We observe a negative dip close to h_c, the magnitude of which increases with the system size. This is in contrast to the TFIM where the Binder cumulant is a monotonic function as shown in the inset.

where the order parameter m and the normalization constants C, D are defined appropriately for a given model so that U_2 has the values 0 and 1 in the thermodynamic limit in the disordered and the ordered phase respectively. For the two-spin TFIM, we have $m^2 = (\frac{1}{L}\sum_i^L \sigma_i^z)^2$ with $C = 3/2$ and $D = -1/2$. For our three-spin model, the order parameter is defined as in the Eq. (27) with $C = 5/2$ and $D = -3/2$ [80]. For the AT model, $m^2 = m_\sigma^2 + m_\tau^2$, where $m_\sigma = (1/L)\sum_{i=1}^L \sigma_i^z$ and $m_\tau = (1/L)\sum_{i=1}^L \tau_i^z$, for which $C = 2$ and $D = -1$ [80]. Furthermore, $\langle O\rangle$ in Eq. (A1) denotes $\langle\psi_0|O|\psi_0\rangle$, where $|\psi_0\rangle$ equals the ground state at a finite size L, and O equals either m^2 or m^4.

We plot the Binder cumulant for the ground state of H_3 in Fig. 18 as a function of the transverse field h using results from ED. As expected they cross close to the critical point for different system sizes. More interestingly, for our model, there is a negative dip in U_2 close to the critical point for $L \geqslant 18$. The dip increases in magnitude as we go to larger system sizes, however it does not increase faster than L; thus the phase transition close to h_c is still continuous in nature [58–60]. However this is starkly different from the monotonic behavior of U_2 for the two-spin case as can be seen in the inset of Fig. 18.

We now show results for the computation of U_2 for longer chains, but with open boundaries, using DMRG both for the three-spin model as well as for the AT model at three values of λ respectively (see Fig. 19). As expected, all the panels show a crossing of U_2 for different L in the neighborhood of the critical point $h_c = 1$. However, only the upper two panels [see Fig. 19(a) for the three-spin model and Fig. 19(b) for the AT model at $\lambda = 1$] show a pseudo-first-order behavior, i.e., nonmonotonic behavior of U_2 as a function of h with increasing L and the corresponding negative dip at sufficiently large L. The behavior of the negative dips is shown more clearly in the insets of both these figures. Figure 19(c) shows the behavior of U_2 for the AT model at $\lambda = 0$ which is equivalent to two decoupled copies of the

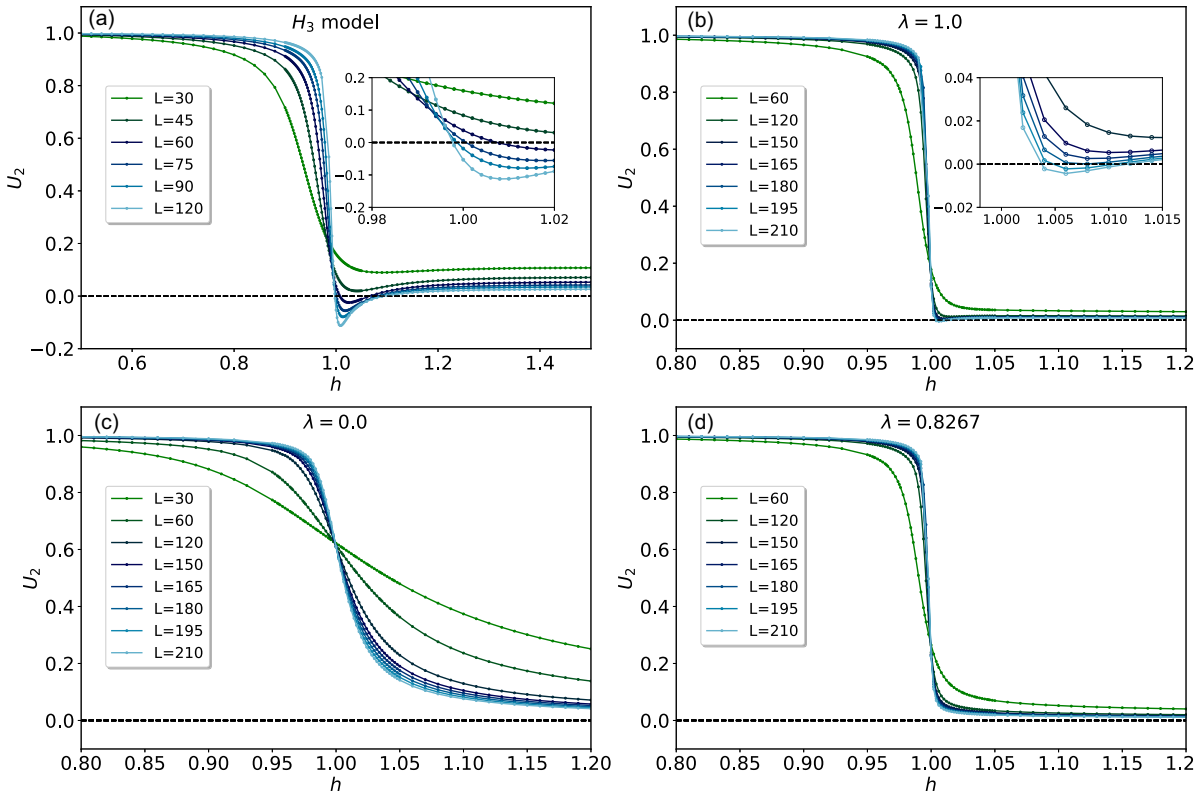

FIG. 19. Behavior of the Binder cumulant U_2 as a function of h for various system sizes L obtained from DMRG on open chains for (a) the three-spin model, and for the AT model at couplings (b) $\lambda = 1.0$, (c) 0, and (d) 0.8267. The insets in (a) and (b) show the development of the negative dips in U_2 in a clearer manner.

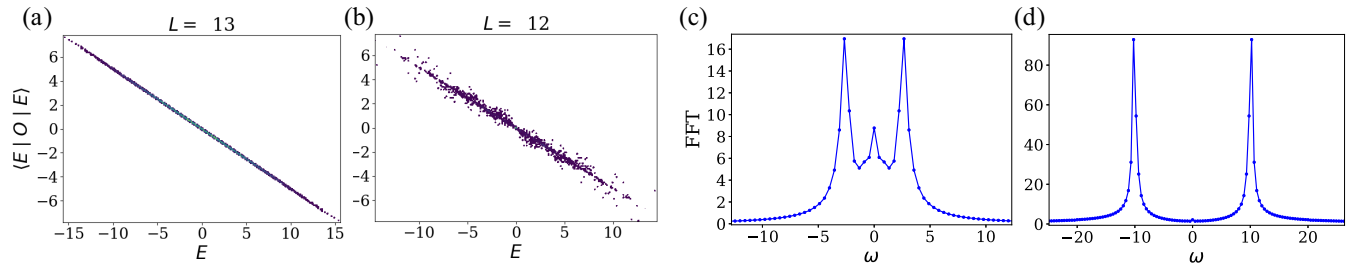

FIG. 20. (a) Expectation value of the operator $\langle\psi_n|X|\psi_n\rangle$ plotted as a function of the energy E_n, where ψ_n is the n-th energy eigenstate, for $h = 1$. We see that for a system size $L = 13$ which is not a multiple of three, the curve falls exactly a straight line with a slope of -0.5. (b) The same plot for a system size $L = 12$ which is a multiple of three. We see that there is a scattering of the date points as the system no longer has exact self-duality. (c) $\tilde{A}^{zz}_{l=1}(\omega)$ at $h = 1$ for a system with $L = 14$. (d) The same quantity at $h = 5$.

TFIM. As expected here, U_2 does not show any nonmonotonic behavior and stays bounded between 0 and 1. More interestingly, the AT model at the coupling $\lambda = 0.8267$, which corresponds to $\nu = 0.7233$, does not show any sign of nonmonotonicity or negative dips as well from the available data with $L \leqslant 210$.

APPENDIX B: EXPECTATION VALUES OF LOCAL OPERATORS AND DUALITY FOR FINITE SYSTEMS

In this Appendix, we will study the expectation values of local operators in all the eigenstates of the Hamiltonian, and we will see that something striking occurs when the system has an exact self-duality. Let us write the Hamiltonian in Eq. (2) in the form shown in Eq. (12). It is then interesting to plot the expectation value of, say, X in the different eigenstates of H versus the energies of those states. If the system is integrable, we might expect to see a fragmented kind of pattern corresponding to the different conserved sectors, while for a nonintegrable system, we would not expect to see any special pattern.

It turns out that something interesting happens at the critical point $h = 1$. We have discussed in Sec. III that the system with L sites and PBC is self-dual only if L is not a multiple of 3. We therefore expect, from Eq. (15), that a plot of $\langle\psi_n|X|\psi_n\rangle$ versus E_n (where n denotes the eigenstate number) should be a perfect straight line with slope equal to $-1/2$ if L is not a multiple of 3. But if L is a multiple of 3, the self-duality does not hold and the plot is not expected to be a perfect straight line; we expect several points to lie away from the straight line. This is exactly what we see in Figs. 20(a) and 20(b). We see a perfect straight line for a system size $L = 13$ where there is exact self-duality but a scattering of points when $L = 12$ where the self-duality is not exact.

APPENDIX C: FOURIER TRANSFORM OF THE AUTOCORRELATOR A^{zz} FOR $h \geqslant 1$

Here we present the plots for $\tilde{A}^{zz}_{l=1}(\omega)$ for $h = 1$ and 5, which are obtained by taking the Fourier transform of $A^{zz}_{l=1}(t)$ at those values of h over a large interval τ. More precisely,

$$\tilde{A}^{zz}_{l=1}(\omega) = \frac{1}{\tau}\int_{\tau_0}^{\tau_0+\tau} dt\; e^{-i\omega t} A^{zz}_{l=1}(t), \tag{C1}$$

where the starting time τ_0 is chosen carefully to eliminate the initial decay so that it can capture the oscillatory nature of the correlator. The time interval τ is taken to be large enough to contain a certain number of complete oscillations which provides a better resolution in the frequency space. Since the oscillations persisted more for larger h, the values of τ also was taken to be different for different values of h. In our case, τ was chosen to be 15 for $h = 1$ and 20 for $h = 5$. The well-defined peaks denote the frequencies of oscillations of the autocorrelator shown in Fig. 17. Moreover, the decays of the oscillations lead to a finite width around the peak of the Fourier transform which goes roughly as $1/h$. This is clear from the figure, as the width is much smaller for $h = 5$ [Fig. 20(d)] than for $h = 1$ [Fig. 20(c)]. The small peak around $\omega = 0$ for $h = 1$ is because of the initial high value of the autocorrelator which adds to a constant value while performing the Fourier transform over a time interval.

[1] P. Pfeuty, Ann. Phys. **57**, 79 (1970).
[2] R. B. Stinchcombe, J. Phys. C **6**, 2459 (1973).
[3] S. Sachdev, *Quantum Phase Transitions* (Cambridge University Press, Cambridge, 1999).
[4] H. A. Kramers and G. H. Wannier, Phys. Rev. **60**, 252 (1941).
[5] R. Savit, Rev. Mod. Phys. **52**, 453 (1980).
[6] P. Francesco, P. Mathieu, and D. Senechal, *Conformal Field Theory* (Springer, 1999).
[7] L. Turban, J. Phys. C **15**, L65 (1982).
[8] A. Maritan, A. Stella, and C. Vanderzande, Phys. Rev. B **29**, 519 (1984).
[9] K. A. Penson, R. Jullien, and P. Pfeuty, Phys. Rev. B **26**, 6334 (1982).
[10] M. Kolb and K. A. Penson, J. Phys. A **19**, L779 (1986).
[11] F. C. Alcaraz and M. N. Barber, J. Phys. A **20**, 179 (1987).
[12] F. Iglói, D. V. Kapor, M. Skrinjar, and J. Sólyom, J. Phys. A **19**, 1189 (1986).
[13] J. K. Pachos and M. B. Plenio, Phys. Rev. Lett. **93**, 056402 (2004).
[14] H. P. Büchler, A. Micheli, and P. Zoller, Nat. Phys. **3**, 726 (2007).
[15] M. Schecter and T. Iadecola, Phys. Rev. B **98**, 035139 (2018).

[16] C.-J. Lin and O. I. Motrunich, Phys. Rev. Lett. **122**, 173401 (2019).
[17] C.-J. Lin, V. Calvera, and T. H. Hsieh, Phys. Rev. B **101**, 220304(R) (2020).
[18] D. Banerjee and A. Sen, Phys. Rev. Lett. **126**, 220601 (2021).
[19] V. Karle, M. Serbyn, and A. A. Michailidis, Phys. Rev. Lett. **127**, 060602 (2021).
[20] S. Biswas, D. Banerjee, and A. Sen, SciPost Phys. **12**, 148 (2022).
[21] H. Bernien, S. Schwartz, A. Keesling, H. Levine, A. Omran, H. Pichler, S. Choi, A. S. Zibrov, M. Endres, M. Greiner, V. Vuletic, and M. D. Lukin, Nature (London) **551**, 579 (2017).
[22] S. Moudgalya, N. Regnault, and B. A. Bernevig, Phys. Rev. B **98**, 235156 (2018).
[23] C. J. Turner, A. A. Michailidis, D. A. Abanin, M. Serbyn, and Z. Papić, Nat. Phys. **14**, 745 (2018).
[24] C. J. Turner, A. A. Michailidis, D. A. Abanin, M. Serbyn, and Z. Papić, Phys. Rev. B **98**, 155134 (2018).
[25] M. Schecter and T. Iadecola, Phys. Rev. Lett. **123**, 147201 (2019).
[26] N. Shibata, N. Yoshioka, and H. Katsura, Phys. Rev. Lett. **124**, 180604 (2020).
[27] G.-X. Su, H. Sun, A. Hudomal, J.-Y. Desaules, Z.-Y. Zhou, B. Yang, J. C. Halimeh, Z.-S. Yuan, Z. Papić, and J.-W. Pan, Phys. Rev. Res. **5**, 023010 (2023).
[28] K. Sanada, Y. Miao, and H. Katsura, Phys. Rev. B **108**, 155102 (2023).
[29] P. Fendley, J. Stat. Mech. (2012) P11020.
[30] P. Fendley, J. Phys. A **49**, 30LT01 (2016).
[31] J. Kemp, N. Y. Yao, C. R. Laumann, and P. Fendley, J. Stat. Mech. (2017) 063105.
[32] D. J. Yates, A. G. Abanov, and A. Mitra, Phys. Rev. Lett. **124**, 206803 (2020).
[33] D. J. Yates, A. G. Abanov, and A. Mitra, Phys. Rev. B **102**, 195419 (2020).
[34] M. Suzuki, Prog. Theor. Phys. **51**, 1992 (1974).
[35] O. F. de Alcantara Bonfim and J. Florencio, Phys. Rev. B **74**, 134413 (2006).
[36] P. Fendley, J. Phys. A **52**, 335002 (2019).
[37] F. C. Alcaraz, R. A. Pimenta, and J. Sirker, Phys. Rev. B **107**, 235136 (2023).
[38] S. Y. Pang, S. V. Muniandy, and M. Z. M. Kamali, Int. J. Theor. Phys. **58**, 4139 (2019).
[39] P. Calabrese and J. Cardy, J. Stat. Mech. (2004) P06002.
[40] P. Chen, Z.-L. Xue, I. P. McCulloch, M.-C. Chung, C.-C. Huang, and S.-K. Yip, Phys. Rev. Lett. **114**, 145301 (2015).
[41] R. Dijkgraaf, E. Verlinde, and H. Verlinde, Commun. Math. Phys. **115**, 649 (1988).
[42] J. Um, S.-I. Lee, and B. J. Kim, J. Korean Phys. Soc. **50**, 285 (2007).
[43] D. Friedan, Z. Qiu, and S. Shenker, Phys. Rev. Lett. **52**, 1575 (1984).
[44] J. Ashkin and E. Teller, Phys. Rev. **64**, 178 (1943).
[45] N. Chepiga, SciPost Phys. Core **5**, 031 (2022).
[46] F. Y. Wu, Rev. Mod. Phys. **54**, 235 (1982).
[47] S. R. White, Phys. Rev. Lett. **69**, 2863 (1992).
[48] U. Schollwöck, Rev. Mod. Phys. **77**, 259 (2005).
[49] M. Fishman, S. R. White, and E. M. Stoudenmire, SciPost Phys. Codebases 4-r0.3 (2022), doi: 10.21468/SciPostPhysCodeb.4-r0.3.
[50] https://itensor.github.io/ITensors.jl/dev/faq/DMRG.html.
[51] P. Pippan, S. R. White, and H. G. Evertz, Phys. Rev. B **81**, 081103(R) (2010).
[52] J. L. Cardy, M. Nauenberg, and D. J. Scalapino, Phys. Rev. B **22**, 2560 (1980).
[53] J. Salas and A. D. Sokal, J. Stat. Phys. **88**, 567 (1997).
[54] A. O'Brien, S. D. Bartlett, A. C. Doherty, and S. T. Flammia, Phys. Rev. E **92**, 042163 (2015).
[55] K. Binder, Z. Phys. B **43**, 119 (1981).
[56] C. G. West, A. Garcia-Saez, and T.-C. Wei, Phys. Rev. B **92**, 115103 (2015).
[57] Y.-C. Wang, Y. Qi, S. Chen, and Z. Y. Meng, Phys. Rev. B **96**, 115160 (2017).
[58] S. Capponi, S. S. Jahromi, F. Alet, and K. P. Schmidt, Phys. Rev. E **89**, 062136 (2014).
[59] K. Vollmayr, J. D. Reger, M. Scheucher, and K. Binder, Z. Phys. B **91**, 113 (1993).
[60] S. Jin, A. Sen, and A. W. Sandvik, Phys. Rev. Lett. **108**, 045702 (2012).
[61] N. D. Chavda, H. N. Deota, and V. K. B. Kota, Phys. Lett. A **378**, 3012 (2014).
[62] Y. Y. Atas, E. Bogomolny, O. Giraud, and G. Roux, Phys. Rev. Lett. **110**, 084101 (2013).
[63] V. Oganesyan and D. A. Huse, Phys. Rev. B **75**, 155111 (2007).
[64] L. D'Alessio, Y. Kafri, A. Polkovnikov, and M. Rigol, Adv. Phys. **65**, 239 (2016).
[65] F. Anza, C. Gogolin, and M. Huber, Phys. Rev. Lett. **120**, 150603 (2018).
[66] R. Reuvers, Proc. R. Soc. A. **474**, 20180023 (2018).
[67] B. Mukherjee, S. Nandy, A. Sen, D. Sen, and K. Sengupta, Phys. Rev. B **101**, 245107 (2020).
[68] S. Sugiura, T. Kuwahara, and K. Saito, Phys. Rev. Res. **3**, L012010 (2021).
[69] B. Mukherjee, A. Sen, D. Sen, and K. Sengupta, Phys. Rev. B **102**, 075123 (2020).
[70] K. Mizuta, K. Takasan, and N. Kawakami, Phys. Rev. Res. **2**, 033284 (2020).
[71] B. Mukherjee, A. Sen, D. Sen, and K. Sengupta, Phys. Rev. B **102**, 014301 (2020).
[72] B. Mukherjee, A. Sen, and K. Sengupta, Phys. Rev. B **106**, 064305 (2022).
[73] We thank Hosho Katsura for an observation which led to the analytical results presented in this section.
[74] C. M. Langlett, Z.-C. Yang, J. Wildeboer, A. V. Gorshkov, T. Iadecola, and S. Xu, Phys. Rev. B **105**, L060301 (2022).
[75] L. Pauling, J. Chem. Phys. **1**, 280 (1933).
[76] Y. Zou, A. Milsted, and G. Vidal, Phys. Rev. Lett. **121**, 230402 (2018).
[77] I. Affleck, D. Gepner, H. J. Schulz, and T. Ziman, J. Phys. A **22**, 511 (1989).
[78] B. Andrade, Z. Davoudi, T. Graß, M. Hafezi, G. Pagano, and A. Seif, Quantum Sci. Technol. **7**, 034001 (2022).
[79] X. Peng, J. Zhang, J. Du, and D. Suter, Phys. Rev. Lett. **103**, 140501 (2009).
[80] A. W. Sandvik, AIP Conf. Proc. **1297**, 135 (2010).